Supplemental Information

Tuning the Structure and Photophysics of a Fluorous Phthalocyanine Platform

*Christopher Farley**[†,‡] N. V. S. Dinesh K. Bhupathiraju,[†] Bianca K. John,[§] Charles Michael Drain*[†,‡,¶,*]

[†]Department of Chemistry, Hunter College of the City University of New York, New York, NY 10065, USA

[‡]Department of Chemistry, The Graduate Center of the City University of New York, New York, NY 10016, USA

[§]Department of Chemistry, Hobart and William Smith Colleges, Geneva, NY 14456, USA

[¶]The Rockefeller University, New York, NY 10065, USA

Distribution of Positional Isomers

In order to analyze how the positional isomers are distributed among the members of the series studied, a custom PHP program was written to enumerate the possibilities. The code first prompts the user to enter the number of positions available for substitution, the number of substituted positions being considered, and the order of the principal axis of rotation. While the

code assumes only one kind of substituent and a dihedral, achiral prismatic symmetry (D_{nh}, where n is input by the user), it can be easily modified to account for multiple substituent types and other molecular point groups. Conceptually, the code consists of two parts. First, it finds every possible permutation of the specified number of substitutions over the specified number of positions. Second, it takes each permutation, applies all of the relevant operations of the symmetry group specified, and checks each result to see if it is duplicated somewhere else in the list. If found, the redundant isomer is deleted, and the program moves on to check the next item in the list.

The process of enumerating every permutation is accomplished by representing the substitution pattern as a binary string (or array, in practice) and applying a previously published algorithm.[1] This can obviously be extended to any number of different types of substituents simply by assigning each substituent type a different numerical value, in which case the string would no longer be binary. The advantage of using an array over a string is that each position in an array can hold an arbitrarily large number, rather than being limited to the ten decimal digits 0 through 9. This allows for a potentially unlimited number of possible substituents, and the search algorithm is general enough to be applied without modification. The only changes necessary would be to prompt the user to enter the numbers of each possible substituent, and to find an alternate way to generate the initial, "non-increasing" multiset array that begins the search. Both of these modifications are trivial.

Modifying the code to account for other molecular point groups is somewhat more challenging. First, the proper symmetry subgroup must be identified. This is the subgroup consisting of all orientation-preserving operations. Thus, it excludes reflections, improper rotations, and other operations that do not correspond to real physical transformations of the molecule. For

metallophthalocyanines with D_{4h} symmetry, the proper symmetry subgroup comprises only the rotations about the principal C_4 axis and the four C_2 axes perpendicular to it. For other symmetry groups, this list of operations would need to be modified accordingly. Moreover, each of these operations is implemented in the code as a transformation acting on a matrix representation of a given isomer. This means that any additional symmetry operations would need to be interpreted in terms of such matrix transformations before being incorporated into the program. While this is less trivial than the other modifications discussed, it is certainly possible given the limited number of point groups that exist.

The following code was written and executed on a Lenovo Yoga 3 Pro with an Intel® 5Y70 1.30 GHz processor and 8 GB RAM, running a 64-Bit version of the Windows 10 Home Operating System. A local Apache HTTP Server (v. 2.4.16) running PHP v. 5.6.12 was implemented via the XAMPP (Control Panel v. 3.2.1) stack. The PHP program was accessed through an HTML form interface embedded in a page named “isomers.php” (identified by the action attribute of the HTML form element), using the Firefox (v. 42) web browser.

```
/*-------Begin code-------*/
<?php
if ( $_SERVER['REQUEST_METHOD'] == 'POST' )
    $posted = true;
else
    $posted = false;
?>

<!DOCTYPE html>
<html>
    <head>
    </head>
    <body>
        <form action="isomers.php" method="post">
            No. of Positions:
            <input type="text" name="positions"
```

```
            value="<?php echo $posted ? $_POST['positions'] : ''; ?>"><br>

            No. of Substitutions:
            <input type="text" name="substitutions"
            value="<?php echo $posted ? $_POST['substitutions'] : ''; ?>"><br>

            Order of Principal Axis of Rotation:
             <input type="text" name="n"
            value="<?php echo $posted ? $_POST['n'] : ''; ?>"><br>

            <input type="submit" value="Submit">
        </form>
        <br>

<?php
if ( ( $posted == true ) AND ( !isset($_POST['positions']) OR !isset($_POST['substitutions'])
    OR !isset($_POST['n']) ) )
    echo "Bad Data Passed!";
elseif ( $posted == true )
{
    $places = $_POST['positions'];
    $subs = $_POST['substitutions'];
    $n = $_POST['n'];

    // Create the "non-increasing" binary multiset list (actually an array).
    // 1 = substituted position, 0 = unsubstituted position
    $array = array();
    for ($i = 0; $i <= $places-1; $i++)
    {
        if ($i < $subs)
            $array[] = 1;
        else
            $array[] = 0;
    }

    //  Initialize values for positions that require comparison (counting starts at 0 for arrays)
    $i = $places - 2;   //  Second-to-last position in the array
    $j = $places - 1;   //  last position in the array

    //  Initialize the master array of all permutations (without regard to symmetry)
    $permutations[0] = $array;

    //  Loop will stop when 2 conditions are BOTH met:
    //    1. $j has reached the final bit position
    //    2. The value of the bit in $j is greater than or equal to the head bit value ($array[0])
    while ( ($j < $places-1) OR ($array[$j] < $array[0]) )
    {
        if ( ($j < $places-1) AND ($array[$i] >= $array[$j+1]) )
```

```
            $k = $j + 1;
        else
            $k = $i + 1;

        //  beforek.next <-- k.next
        //  First rearrangement of actual multiset array
        //  Store the bit in position k first
        $kvalue = $array[$k];
        //  Also store the head bit for later comparison
        $headvalue = $array[0];
        //  Then remove the kth bit and reindex the following bits
        unset($array[$k]);
        $array = array_values($array);

        //  Then push the k value onto the beginning of the stack
        //  and reset the $k variable
        //  k.next <-- head
        array_unshift($array,$kvalue);
        $k = 0;
        //  This also requires pushing up the i index
        $i++;

        if ($kvalue < $headvalue)
            $i = $k;
        $j = $i + 1;

        //  Push this binary representation onto the master array
        $permutations[] = $array;
}
echo "Done. ".count($permutations)." total permutations, including duplicate structures.<br>\r\n";

//  We will need to split each array representation into n segments,
//  where n is the order of the principal axis, defined by the user
//  $groupNo will be the length of each segment
$groupNo = $places/$n;

//  Set the begin and end points for the search through the master $permutations array
$key = 0;
$number = count($permutations);

set_time_limit(500);
while ($key < $number)
{
    if (isset($permutations[$key]))
    {
        //  Create a 2 dimensional array of n rows, each $groupNo long
        for ($i = 0; $i <= $n-1; $i++)
            $isomer[$i] = array_slice($permutations[$key], $groupNo*$i, $groupNo);
```

```
        // $isomer now holds a matrix representation of the isomer that we are testing,
        // which will need to be manipulated to check if it is identical to any other isomers
        // in the list. Since we are considering the proper symmetry subgroup,
        // we only need to deal with rotations that are relevant to the molecular point group.
        // We are here assuming a dihedral, achiral point group, D_nh, where the user supplies
        // the order of the principal rotational axis, n (n=4 for metallophthalocyanines).
        // We will need to step through n rotations about the principal axis, and for each,
        // we also need to take a 180 degree rotation about a single C2 axis within the
        // symmetry plane. This is equivalent to taking separate 180 degree rotations of
        // the original isomer about each of the n C2 axes perpendicular to Cn.

        for ($rotation = 1; $rotation <= $n; $rotation++)
        {
            // Apply a (360/n) degree rotation by cycling the rows of the $isomer array
            $lastrow = array_pop($isomer);
            array_unshift($isomer, $lastrow);
            // Rebuild a one line array to compare to other entries in the master permutations list
            $isoarray = array();
            foreach ($isomer as $isokey=>$row)
                $isoarray = array_merge($isoarray,$row);
            // check if isoarray matches any other values in the master permutations list
            $foundkeys = array_keys($permutations, $isoarray, TRUE);
            if ( (count($foundkeys) > 1) OR ( (count($foundkeys) == 1)
            AND ($foundkeys[0] != $key) ) )
            {
                // Delete the duplicate entries in the $permutations array
                foreach ($foundkeys as $duplicatekey)
                    unset($permutations[$duplicatekey]);
            }

            // And check a 180 degree rotation of this about a C2 axis, just by reversing the array
            $isoarray = array_reverse($isoarray);
            // check if isoarray matches any other values in the master permutations list
            $foundkeys = array_keys($permutations, $isoarray, TRUE);
            if ( (count($foundkeys) > 1) OR ( (count($foundkeys) == 1)
            AND ($foundkeys[0] != $key) ) )
            {
                // Delete the duplicate entries in the $permutations array
                foreach ($foundkeys as $duplicatekey)
                    unset($permutations[$duplicatekey]);
            }
        }
        unset($isomer);
    }

    // Move on to the next permutation
    $key++;
}
```

```
    //  Quote the results and list the binary representations of the isomers found
    echo "Done filtering. ".count($permutations)." unique structures found.<br>\r\n";
    foreach ($permutations as $row)
    {
        foreach ($row as $bit)
            echo $bit;

        echo "<br>\r\n";
    }
}
?>
    </body>
</html>
/*-------End code-------*/
```

Figure S1 shows plots of the results obtained from running the program for two different cases. The total number of permutations and the number of unique isomers are plotted as functions of the number of substituents. If all sixteen fluorines on the $ZnF_{16}Pc$ can be substituted with equal probability, the distribution will resemble that in Figure S1A, with $ZnF_8(SR)_8Pc$ having the maximum number (1,654) of unique isomers. In order to determine the distribution for the restricted case, in which the β fluorines are substituted first, we ignore the α fluorines and input "8" as the number of possible positions into the program prompt, while retaining the D_{4h} symmetry. This data is shown in Figure S1B, with two maxima occurring at just 13 unique isomers for both $ZnF_{12}(SR)_4Pc$ and $ZnF_4(SR)_{12}Pc$. As one check of the validity of the program, we note that the total number of permutations for any given number of substituents, n, should be ${}_{16}C_n = 16!/[n!\,(16-n)!]$ for the unrestricted case, and ${}_8C_n = 8!/[n!\,(8-n)!]$ for the restricted case, and these calculated values match the program output exactly.

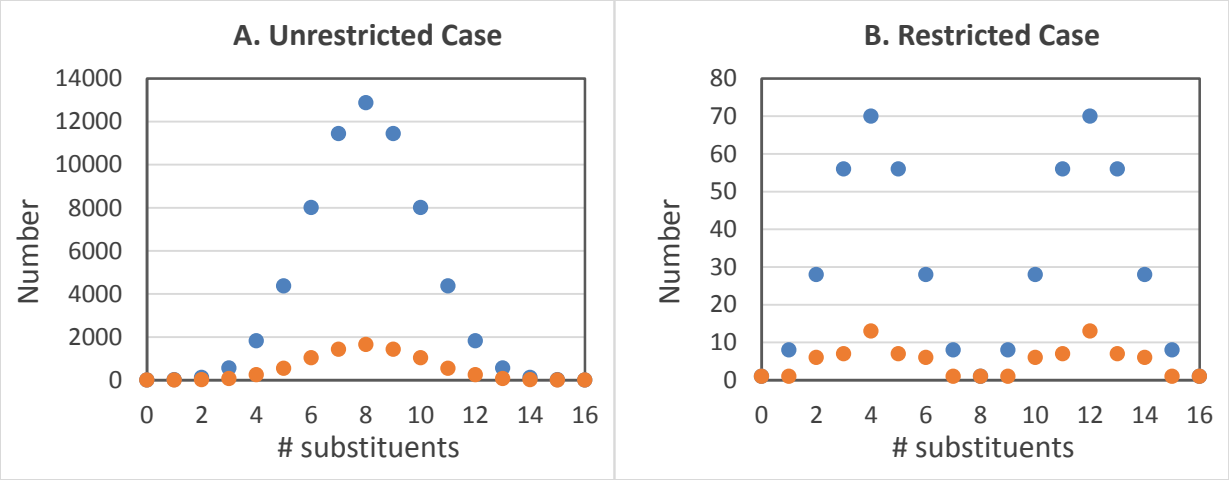

Figure S1. The total number of permutations (•) and the number unique isomers (•) as a function of the number of substituents, for two different mechanistic assumptions: (A) The unrestricted case assumes that all sixteen positions react with equal probability, and (B) The restricted case assumes that all eight β positions react with equal probability, before any of the eight α positions react. Note the difference in the vertical scales.

Oxidative Decomposition

Purification and separation of the crude reaction mixtures proved to be difficult, due primarily to the ease with which thioethers can oxidize into sulfoxides and sulfones. This is indicated by the differences in TLCs of purified products upon standing in air, wherein the R_f, were reduced essentially to zero, indicating near quantitative conversion into a highly polar product. The UV-Vis absorbance spectra of these spots also showed distinct changes, including a splitting of the Q-band and an increase in the band at the blue edge near 640 nm. To verify this conclusion, a small sample of $ZnF_{13}(SR)_3Pc$ was freshly purified by TLC and then subjected to oxidative conditions by dissolving in glacial acetic acid with four equivalents of 30% hydrogen peroxide

per thioalkane group, and the solution was stirred at room temperature. These conditions were reported to convert alkyl phenyl sulfides into the corresponding sulfoxides in high yield.[2] After two hours, UV-Vis spectroscopy of the reaction mixture was almost identical to those observed in the unknown polar products, confirming that they were indeed sulfoxides. Consequently, TLC was used for most separations, and the compounds were kept under nitrogen at low temperatures.

UV-Vis Spectroscopy

Solution phase UV-Vis absorbance spectra were obtained on a Lambda 35 spectrophotometer operating in single beam mode. The monochromator bandwidth was set to 1 nm to match the excitation monochromator settings of the fluorescence spectrometer. All spectra were obtained from dilute solutions in either quartz or special optical glass cuvettes using freshly distilled or spectroscopic grade solvents. For extinction coefficient measurements, samples of each Pc were accurately weighed and dissolved into a known volume of distilled THF. This solution was then titrated into a THF blank to record spectra at multiple concentrations and construct calibration curves according to the Beer-Lambert equation (Eq. 1).

$$A = \varepsilon l[Pc] \qquad (1)$$

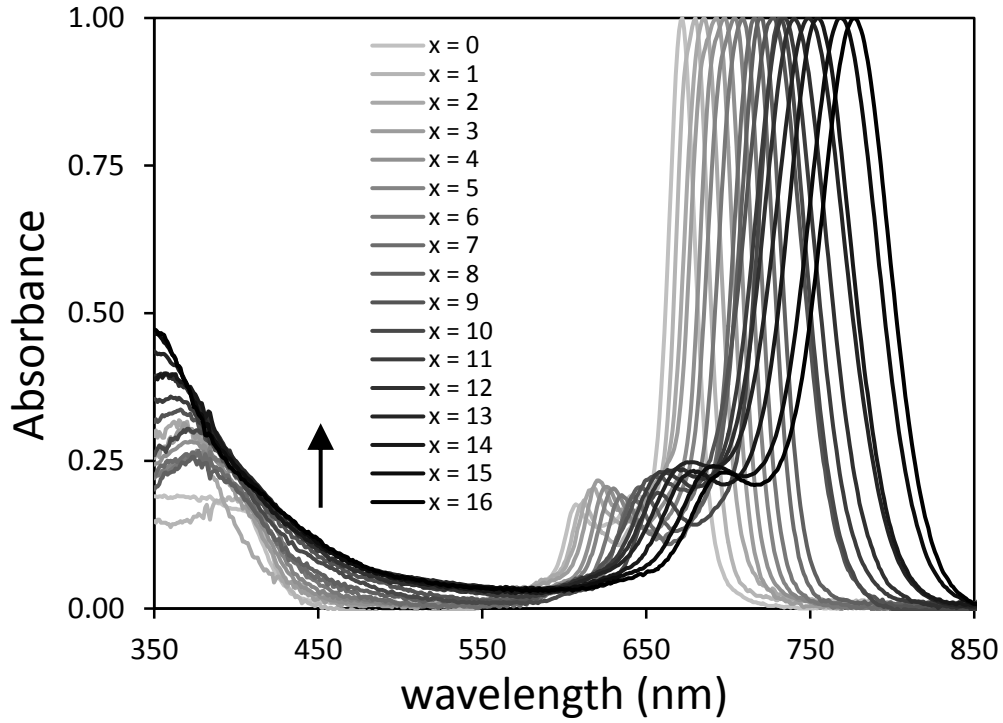

Figure S2. Expanded, normalized UV-Vis spectra of all compounds $ZnF_{16-x}(SR)_xPc$ (x = 0 to 16) in freshly distilled THF. The arrow indicates the increase in the high energy absorbance with increasing thioalkyl substitution and the corresponding changes in the molecular orbitals as described in the text.

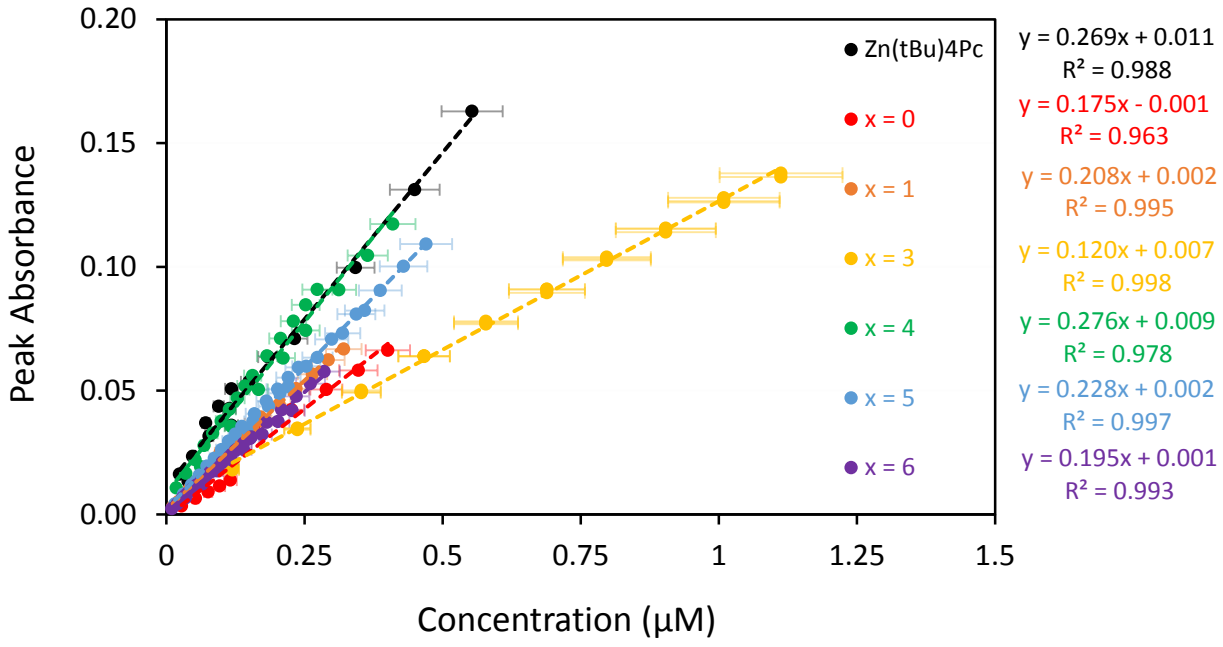

Figure S3. Calibration curves of the compounds Zn(*t*Bu)$_4$Pc and ZnF$_{16-x}$(SR)$_x$Pc for x = 0, 1, 3, 4, 5 and 6. Linearity over the concentration range is consistent with the application of the Beer-Lambert Law. The slopes given on the right are the extinction coefficients in units of $(\mu M \cdot cm)^{-1}$.

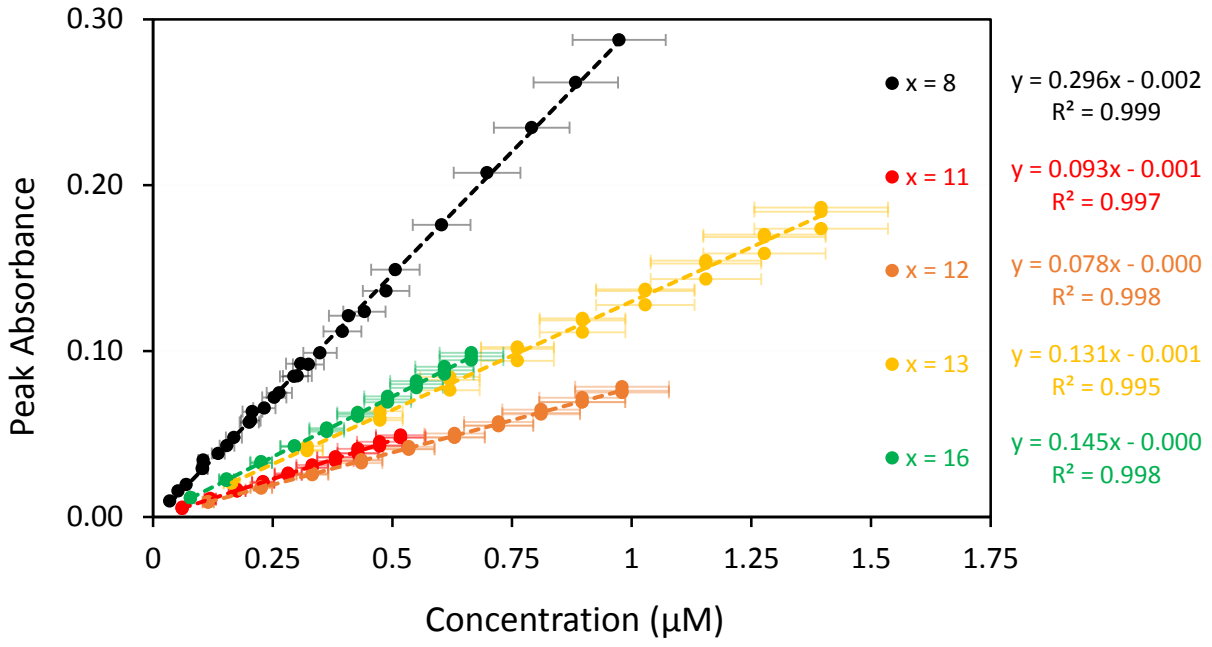

Figure S4. Calibration curves of the compounds $ZnF_{16-x}(SR)_xPc$ for x = 8, 11, 12, 13 and 16. Linearity over the concentration range is consistent with the application of the Beer-Lambert Law. The slopes given on the right are the extinction coefficients in units of $(\mu M \cdot cm)^{-1}$.

Fluorescence Spectroscopy

Steady state fluorescence emission spectra, quantum yield comparisons, and fluorescence lifetime measurements were made using right-angle detection mode with the excitation monochromator bandwidth set to 1 nm. Excitation spectra were obtained in the same configuration with the monochromator bandwidths reversed. For both steady state and lifetime experiments, all solutions were degassed with dry nitrogen for 2 to 3 minutes immediately prior to data collection. Monochromator bandwidths were sometimes increased as necessary to improve signal-to-noise ratios, but were always kept consistent between samples and standards

for comparison purposes and quantum yield calculations. In order to minimize inner filter effects, solutions for right angle measurement were diluted so that the absorbance remained below 0.1 for all wavelengths. Quantum yields, ϕ_f, were calculated using a relative gradient method according to Eq. 2.

$$\phi_f = \phi_r \left(\frac{\nabla F}{\nabla F_r}\right)\left(\frac{n}{n_r}\right)^2 \qquad (2)$$

The ∇F term is the gradient of a plot of integrated fluorescence intensity vs. absorbance at the excitation wavelength for each compound. The last term is a correction for the respective indices of refraction, *n*, of the solvents used for the sample and reference solutions. The subscript, *r*, indicates a quantity corresponding to the reference solution. Thus, ϕ_r is the quantum yield of the standard obtained from the literature. To obtain the ∇F values, multiple solutions of each compound were prepared at varying concentrations, and emission spectra were taken for each. Zn(*t*Bu)$_4$Pc in deaerated toluene was used as standard, with ϕ_r = 0.081.[3]

It is not clear why there is an anomalously high value for the quantum yield of ZnF$_{16}$Pc in the literature (see main text).[4] The higher concentration reported would tend to increase aggregation and thus decrease the apparent quantum yield by artificially inflating the measured absorbance at the excitation wavelength quoted (660 nm). Indeed, the authors cite this as the reason for the reduction of the quantum yield between ZnPc and ZnF$_{16}$Pc, stating that aggregation prevails in the latter. However, our own studies indicate that there is a real decrease by the same factor between these two for a series of dilute THF solutions in which there is no evidence of aggregation. It is thus much more likely that the inflated literature value for ZnF$_{16}$Pc is a consequence of the artificially high value of the ZnPc quantum yield they used as a standard.

Linearity of the plots of florescence intensity *vs*. absorbance at λ_{ex} was used as a criteria to judge the extent of aggregation. For compounds $ZnF_{16}Pc$, $ZnF_{15}(SR)Pc$, $ZnF_{14}(SR)_2Pc$, and $ZnF_{13}(SR)_3Pc$, there was a noticeable curvature in these plots. This was accompanied by the observation of increasing absorbance bands near 635, 642, 649, and 655 nm, respectively. These bands are commonly attributed to the absorbance of dark (*i.e.* non-emissive) aggregates. Since they overlap the excitation wavelengths used for fluorescence, their contribution needed to be subtracted from the absorbance used to calculate the quantum yield. To account for this, the lineshape of the most dilute, least aggregated solution of each compound was scaled to the peak maximum of the spectra for the other concentrations, and the absorbance of the newly scaled spectra at the excitation wavelength was used in Eq. 2. Performing this correction on these four compounds effectively restored the linear relationship between fluorescence intensity and absorbance in all cases.

For lifetime measurements a dilute solution of colloidal silica (LUDOX, Sigma) in deionized water was used to produce the instrument response function (IRF). Dilute samples and narrow slit bandwidths were preferred to give slower collection rates over longer periods of time. This reduces the so-called "pulse pile-up effect" that would otherwise skew the counting statistics towards earlier photon detection events and therefore shorter lifetimes. All of the measured decays were fit reasonably well with a single lifetime parameter, except as noted in Table 1 in the main text. The only exceptions to this required a minor second lifetime parameter very close to the IRF width, which is likely to be a scattering artifact. The fits obtained were judged based on a combination of the χ^2 value and visual inspection of the plotted residuals. Lifetimes were recorded for each compound at several different concentrations over the range studied, and multiple fits were performed on each decay spectrum using different boundaries to ensure

numerical stability. The separate numerical fits for each concentration were averaged together and then plotted as a function of concentration (Figure S5) to ensure that they remained constant over the range of interest. Finally, the results for each compound were averaged together over all fits and all concentrations to give the lifetime values quoted in Table 1 in the main text.

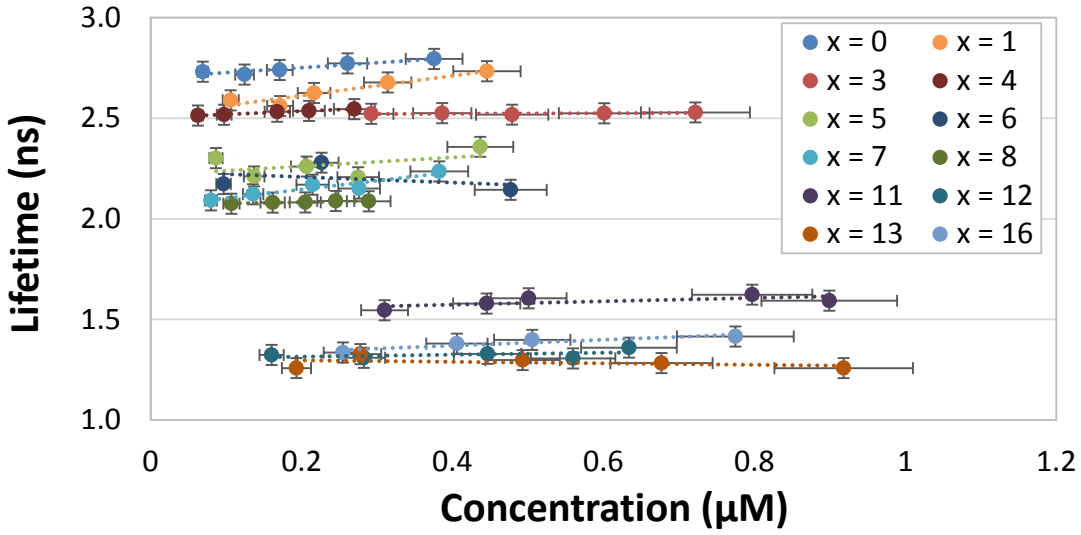

Figure S5. Lifetimes for each compound $ZnF_{16-x}(SR)_xPc$ (x = 0 to 16) *vs*. concentration, demonstrating that they remain constant over the range investigated. Concentrations were calculated from the absorbance spectra of the solutions and the extinction coefficients that were obtained in a separate set of experiments. Horizontal error bars indicate a ±10% uncertainty in the concentration as a consequence of the uncertainty in the extinction coefficient. Vertical error bars correspond to instrumental uncertainties of ±50 ps.

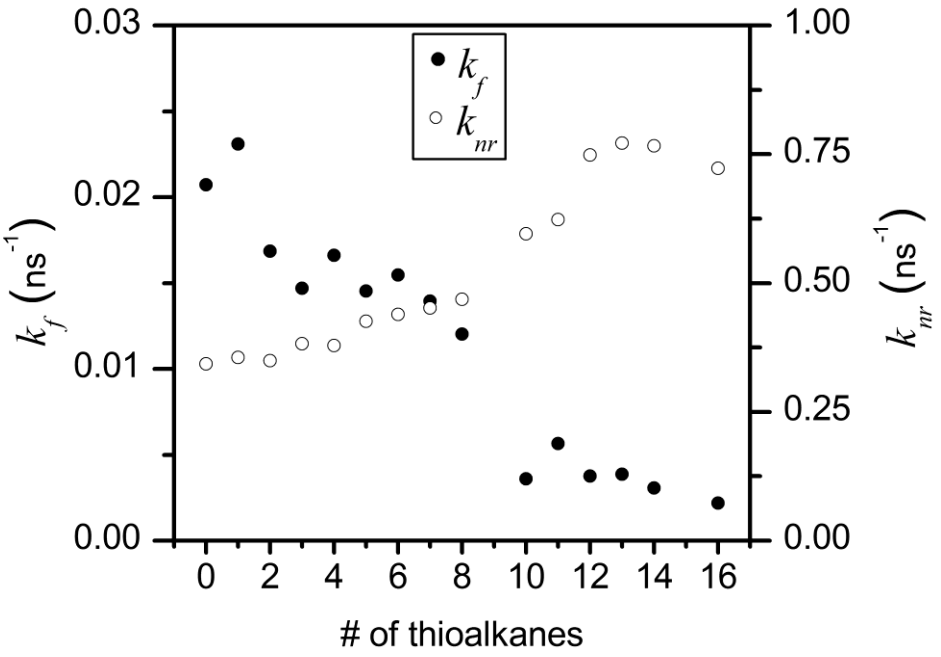

Figure S6. Fluorescence and non-radiative rate constants (k_f and k_{nr}, respectively) for compounds $ZnF_{16-x}(SR)_xPc$ (x = 0 to 16) in THF. Note the different scales of the left and right axes for the different constants.

octylthiopentadecafluorophthalocyaninato zinc(II), $ZnF_{15}(SR)Pc$

$ZnF_{15}(SR)Pc$ was synthesized according to the above procedure using 30 mg $ZnF_{16}Pc$ (0.035 mmol), 0.1 mL 1-octanethiol (0.58 mmol), and 100 mg K_2CO_3 (0.72 mmol) in 10 mL dry THF. The reaction was run at 50° C for 1 hour. The blue-green solid Pc mixture obtained from the column was separated by TLC using a 6:4 mixture of hexanes to ethyl acetate. Yield: 43% (15 mg, 0.015 mmol). ^{1}H NMR ($(CD_3)_2CO$, 500 MHz): δ 0.82-0.97 (m, 3H, CH_3), 1.17-1.83 (m, 12H, CH_2), 2.51-2.73 (m, 2H, SCH_2). ^{19}F NMR ($(CD_3)_2CO$, 376.5 MHz): δ -141.90 (br, 7F, β), -153.46 (br, 8F, α). MALDI-TOF MS: m/z 990.96 (65%, $[M+H]^+$), 877.71 (100%, $[M-(CH_2)_7CH_3]^+$); calculated for $[ZnF_{15}(SR)Pc+H]^+$ 991.04. UV-Vis (in THF): λ_{max}/nm 679 (log ε 5.32), 612 (4.58), 401 (4.58).

bis(octylthio)tetradecafluorophthalocyaninato zinc(II), $ZnF_{14}(SR)_2Pc$

UV-Vis (in THF): λ_{max}/nm 686, 618, 369.

tris(octylthio)triskadecafluorophthalocyaninato zinc(II), $ZnF_{13}(SR)_3Pc$

$ZnF_{13}(SR)_3Pc$ was synthesized according to the above procedure using 65.5 mg $ZnF_{16}Pc$ (0.076 mmol), 0.04 mL 1-octanethiol (0.23 mmol), and 165 mg NaH (6.88 mmol) in 2 mL dry THF. The reaction was run at room temperature for 10 min. The green solid Pc mixture obtained from the column was separated by TLC using a 8:2 mixture of hexanes to ethyl acetate. MALDI-TOF MS: m/z 1244.88 (100%, $[M+H]^+$), 1146.70 (8%, $[M-(CH_2)_7CH_3+O]^+$); calculated for $[ZnF_{13}(SR)_3Pc+H]^+$ 1244.24. UV-Vis (in THF): λ_{max}/nm 692 (log ε 5.08), 620 (4.41), 369 (4.57).

tetrakis(octylthio)dodecafluorophthalocyaninato zinc(II), $ZnF_{12}(SR)_4Pc$

$ZnF_{12}(SR)_4Pc$ was synthesized according to the above procedure using 60 mg $ZnF_{16}Pc$ (0.069 mmol), 0.4 mL 1-octanethiol (2.3 mmol), and 200 mg K_2CO_3 (1.4 mmol) in 20 mL dry THF. The reaction was run at 50° C for 4 hours. The green solid Pc mixture obtained from the column was separated by TLC using a 9:1 mixture of hexanes to ethyl acetate. Yield: 24% (22.4 mg, 0.016 mmol). ^1H NMR ($CDCl_3$, 500 MHz): δ 0.81-0.91 (m, 12H, CH_3), 1.18-1.57 (m, 48H, CH_2), 3.17-3.36 (m, 8H, SCH_2). ^{19}F NMR ($CDCl_3$, 376.5 MHz): δ -108.86 (br, 4F, β), -122.65 (br, 4F, α), -142.47 (br, 4F, α). MALDI-TOF MS: m/z 1370.29 (100%, $[M]^+$), 1496.38 (10%, $[ZnF_{11}(SR)_5Pc]^+$); calculated for $[ZnF_{12}(SR)_4Pc]^+$ 1370.35. UV-Vis (in THF): λ_{max}/nm 698 (log ε 5.44), 626 (4.75), 372 (4.89).

pentakis(octylthio)undecafluorophthalocyaninato zinc(II), $ZnF_{11}(SR)_5Pc$

$ZnF_{11}(SR)_5$ was isolated from the same reaction as $ZnF_{12}(SR)_4Pc$ above. Yield: 26% (27.0 mg, 0.018 mmol). ^1H NMR ($CDCl_3$, 500 MHz): δ 0.83-0.91 (m, 15H, CH_3), 1.17-1.67 (m, 60H, CH_2), 3.25-3.70 (m, 10H, SCH_2). ^{19}F NMR ($CDCl_3$, 376.5 MHz): δ -109.09 (br, 6F, α), -123.07

(br, 3F, β), -142.57 (br, 2F, α). MALDI-TOF MS: m/z 1496.37 (100%, $[M]^+$), 1622.47 (15%, $[ZnF_{10}(SR)_6Pc]^+$); calculated for $[ZnF_{11}(SR)_5Pc]^+$ 1496.46. UV-Vis (in THF): λ_{max}/nm 704 (log ε 5.36), 630 (4.67), 378 (4.77).

hexakis(octylthio)decafluorophthalocyaninato zinc(II), $ZnF_{10}(SR)_6$

$ZnF_{10}(SR)_6$ was isolated from the same reaction mixture as $ZnF_{12}(SR)_4Pc$ above. Yield: 19% (21.1 mg, 0.013 mmol). ^1H NMR ($CDCl_3$, 500 MHz): δ 0.82-0.95 (m, 18H, CH_3), 1.18-1.57 (m, 72H, CH_2), 3.17-3.36 (m, 12H, SCH_2). ^{19}F NMR ($CDCl_3$, 376.5 MHz): δ -109.13 (bs, 4F, α), -123.22 (bs, 2F, β), -142.38 (bs, 4F, α). MALDI-TOF MS: m/z 1623.44 (100%, $[M]^+$), 1749.52 (7%, $[ZnF_9(SR)_7Pc]^+$); calculated for $[ZnF_{10}(SR)_6Pc]^+$ 1623.57. UV-Vis (in THF): λ_{max}/nm 708 (log ε 5.29), 635 (4.57), 382 (4.69).

heptakis(octylthio)nonafluorophthalocyaninato zinc(II), $ZnF_9(SR)_7Pc$

$ZnF_9(SR)_7Pc$ was synthesized according to the above procedure using 60 mg $ZnF_{16}Pc$ (0.069 mmol), 0.6 mL 1-octanethiol (3.5 mmol), and 200 mg K_2CO_3 (1.4 mmol) in 20 mL dry THF. The reaction was refluxed for 8 hours. The green solid Pc mixture obtained from the column was separated by TLC using a 9.4:0.6 mixture of hexanes to ethyl acetate. Yield: 17% (21.4 mg, 0.012 mmol). ^1H NMR ($CDCl_3$, 500 MHz): δ 0.75-0.85 (m, 21H, CH_3), 1.19-1.65 (m, 84H, CH_2), 3.00-3.50 (m, 14H, SCH_2). ^{19}F NMR ($CDCl_3$, 376.5 MHz): δ -91.10 (s, 1F, α), -91.85-92.05 (m, 2F, α/ β), -93-93.5 (m, 6F, α). MALDI-TOF MS: m/z 1749.54 (100%, $[M]^+$), 1875.64 (17%, $[ZnF_8(SR)_8Pc]^+$); calculated for $[ZnF_9(SR)_7Pc]^+$ 1749.68. UV-Vis (in THF): λ_{max}/nm 716 (log ε 5.46), 642 (4.73), 372 (4.87).

octakis(octylthio)octafluorophthalocyaninato zinc(II), $ZnF_8(SR)_8Pc$

$ZnF_8(SR)_8Pc$ was isolated from the same reaction mixture as $ZnF_9(SR)_7Pc$ above. Yield: 25% (31.4 mg, 0.017 mmol). ^1H NMR ($CDCl_3$, 500 MHz): δ 0.75-0.85 (m, 24H, CH_3), 1.15-1.92 (m,

96H, CH_2), 3.27-3.51 (m, 16H, SCH_2). ^{19}F NMR ($CDCl_3$, 376.5 MHz): δ -91.17 (s, 1F, β), -92.06 (s, 4F, α), -92.34-93.74 (m, 3F, α). MALDI-TOF MS: m/z 2002.11 (6%, $[ZnF_7(SR)_9Pc]^+$), 1876.01 (100%, $[M]^+$), 1779.86 (17%, $[M-(CH_2)_7CH_3+O]^+$), 1763.84 (14%, $[M-(CH_2)_7CH_3]^+$), 1749.87 (11%, $[ZnF_9(SR)_7Pc]^+$); calculated for $[ZnF_8(SR)_8Pc]^+$ 1875.78. UV-Vis (in THF): λ_{max}/nm 720 (log ε 5.47), 645 (4.78), 374 (4.88).

nonakis(octylthio)heptafluorophthalocyaninato zinc(II), $ZnF_7(SR)_9Pc$

UV-Vis (in THF): λ_{max}/nm 727, 656, 366.

decakis(octylthio)hexafluorophthalocyaninato zinc(II), $ZnF_6(SR)_{10}Pc$

MALDI-TOF MS: m/z 2129.72 (100%, $[M]^+$); calculated for $[ZnF_6(SR)_{10}Pc]^+$ 2129.99. UV-Vis (in THF): λ_{max}/nm 731, 657, 371.

undecakis(octylthio)pentafluorophthalocyaninato zinc(II), $ZnF_5(SR)_{11}Pc$

MALDI-TOF MS: m/z 2255.28 (100%, $[M+H]^+$), 2160.12 (16%, $[M-(CH_3)_7CH_3+O+H]^+$); calculated for $[ZnF_5(SR)_{11}Pc+H]^+$ 2255.10. UV-Vis (in THF): λ_{max}/nm 733 (log ε 4.97), 660 (4.33), 364 (4.52).

dodecakis(octylthio)tetrafluorophthalocyaninato zinc(II), $ZnF_4(SR)_{12}Pc$

MALDI-TOF MS: m/z 2382.28 (100%, $[M+H]^+$), 2255.13 (37%, $[ZnF_5(SR)_{11}+H]^+$); calculated for $[ZnF_4(SR)_{12}Pc+H]^+$ 2382.21. UV-Vis (in THF): λ_{max}/nm 740 (log ε 4.89), 669 (4.27), 358 (4.49).

triskadecakis(octylthio)trifluorophthalocyaninato zinc(II), $ZnF_3(SR)_{13}Pc$

^1H NMR ($CDCl_3$, 500 MHz): δ 0.78-0.92 (m, 39H, CH_3), 0.95-1.85 (m, 156H, CH_2), 3.15-3.58 (m, 26H, SCH_2). MALDI-TOF MS: m/z 2634.40 (24%, $[ZnF_2(SR)_{14}Pc+H]^+$), 2508.29 (100%, $[M+H]^+$), 2382.18 (38%, $[ZnF_4(SR)_{12}Pc+H]^+$), 2254.06 (10%, $[ZnF_5(SR)_{11}Pc+H]^+$); calculated for $[ZnF_3(SR)_{13}Pc+H]^+$ 2508.31. UV-Vis (in THF): λ_{max}/nm 749(log ε 5.12), 677 (4.51).

tetradecakis(octylthio)difluorophthalocyaninato zinc(II), $ZnF_2(SR)_{14}Pc$

^1H NMR ($CDCl_3$, 500 MHz): δ 0.75-0.85 (m, 42H, CH_3), 1.05-1.90 (m, 168H, CH_2), 3.15-3.55 (m, 28H, SCH_2). MALDI-TOF MS: m/z 2633.97 (100%, $[M]^+$), 2507.86 (28%, $[ZnF_3(SR)_{13}Pc]^+$); calculated for $[ZnF_2(SR)_{14}Pc]^+$ 2633.41. UV-Vis (in THF): λ_{max}/nm 755, 679, 357.

pentadecakis(octylthio)monofluorophthalocyaninato zinc(II), $ZnF(SR)_{15}Pc$

UV-Vis (in THF): λ_{max}/nm 768, 691.

hexadecakis(octylthio)phthalocyaninato zinc(II), $Zn(SR)_{16}Pc$

Sodium metal (300 mg) was added to 25 mg of $ZnF_{16}Pc$ (0.029 mmol) in 40 mL of diglyme and stirred until the Na dissolved. Then, 3.5 mL of 1-octanethiol (0.013 mol) was added under N_2 at room temperature. The resulting mixture was heated to 100 °C and stirred for 16 hours. The reaction was then cooled to room temperature and poured into 300 mL of water. The product was extracted with diethyl ether (3 × 20 mL), dried over Na_2SO_4, and concentrated under reduced pressure. Silica gel chromatography (2 × 8 in) with hexane followed by hexane/ethyl acetate (30:1 v:v) yielded 50 mg (0.013 mmol) of the product (44% yield). MALDI-TOF MS: m/z 2887.16 (100%, $[M]^+$), 2793.12 (18%, $[ZnF_3(SR)_{13}Pc]^+$); calculated for $[Zn(SR)_{16}Pc]^+$ 2887.64. UV-Vis (in THF): λ_{max}/nm 777 (log ε 5.16), 697 (4.52).

MALDI-TOF Mass Spectrometry

After being separated chromatographically, each individual Pc was prepared for MALDI-TOF analysis using a DHB matrix and a THF/water/TFA mixture as the solvent. The MALDI spectra obtained are shown in Figure S7 through Figure S20. For each compound there is a strong peak corresponding to the intact molecular cation, either protonated ($[M+H]^+$) or oxidized ($[M]^+$). In some cases additional minor peaks are observed. These are attributed to either contamination by a small amount of a different substitution product, oxidized byproducts of the expected Pc, fragment ions in which one or more sulfide chains have been cleaved, or some combination of these three. In some spectra we observed small peaks between 600 and 800 amu which are likely due to fragmentation of the Pc macrocycle itself. Increasing the laser power generally caused these peaks to become more significant, confirming that they are due to fragmentation occurring during the laser ablation.

All of the mass spectra obtained are shown below along with tables listing the assignments of the most prominent peaks. For some of the sample, there is a cluster of small molecular weight fragments around 600 Daltons. This cluster likely corresponds to ionic fragments of the parent molecule, and has been cut out of most of the given spectra for clarity. The x-axis (m/z) is scaled differently for each compound in order to show all of the observed peaks in as much detail as possible, but no higher mass fragments have been excluded from the data shown.

Except for the $ZnF_{16}Pc$ standard, each spectrum is followed by a table of peak assignments. Each peak cluster in the spectrum is labelled by the most abundant mass, and the table gives a

proposed structure and the corresponding observed and expected mass ranges. In each chart, the structure of the primary intact molecular ion is given in red. The abbreviated notation includes the number of fluorine atoms, F_n, followed by $(16 - n)$ different possible substituents. $(SR)_x$ indicates x octylthio chains, while $(SH)_y$ indicates y chains in which the octyl portion has been cleaved off, leaving behind a thiol. H_z denotes z similar cleavages, except that the sulfur atom has been removed with the octyl chain, the entire group being replaced by an H attached directly to the Pc core. O_m may also be included to indicate that one or more of the sulfur groups has been oxidized. Although it is not possible to establish the precise nature or locus of oxidation through MALDI, a pattern emerges in which an oxygen is almost always accompanied by the presence of a thiol group. This suggests that oxidation occurs by the conversion of thiol (–SH) to sulfenic acid (–SOH) subsequent to fragmentation.

For every possible proposed structure, $n + x + y + z = 16$, necessarily, and $m \leq 2(x + y)$ since only sulfur atoms can be oxidized in this case. Finally, the "-H" or "+H" terms are used when the mass more closely corresponds to a deprotonated anion or protonated cation, depending on the detection mode. However, given the resolution of the instrument, the usage is somewhat arbitrary. As an example, the structure denoted $[ZnF_9(SR)_3(SH)_4Pc+H]^+$ refers to a protonated fragment of a $ZnF_9(SR)_7Pc$ molecule in which four octyl chains have been cleaved, leaving behind four thiols and three intact octylthio groups.

From the UV-Vis spectroscopy and TLC analysis, it appears that all of these compounds are stable in solution over the timescale of the mass spec analysis. Thus, it is likely that these fragmentations occur during the laser ablation. This is further corroborated by the fact that the relative intensity of the fragmentation peaks was observed to increase with increasing laser power.

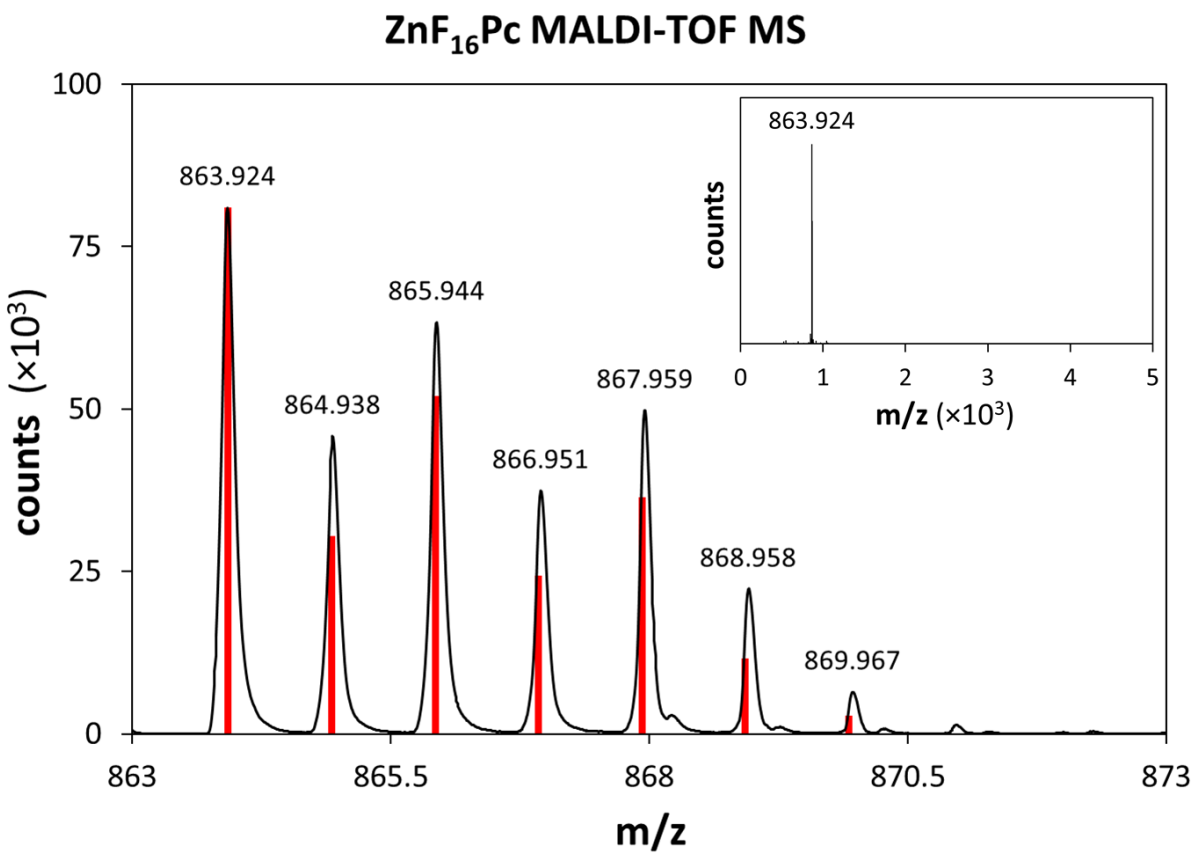

Figure S7. Mass spectrum of $ZnF_{16}Pc$ in a DHB matrix. An expanded view of the region immediately surrounding the detected ion peak $[ZnF_{16}Pc]^+$. The black trace is the experimental data obtained in positive ion detection mode. The vertical red lines correspond to the expected theoretical isotopic distribution, calculated using ChemBioDraw Ultra 14.0 and scaled to the highest observed peak. The inset shows the full spectrum over the entire mass range observed, from 0 to 5000 Daltons, with no other ions or fragments visible.

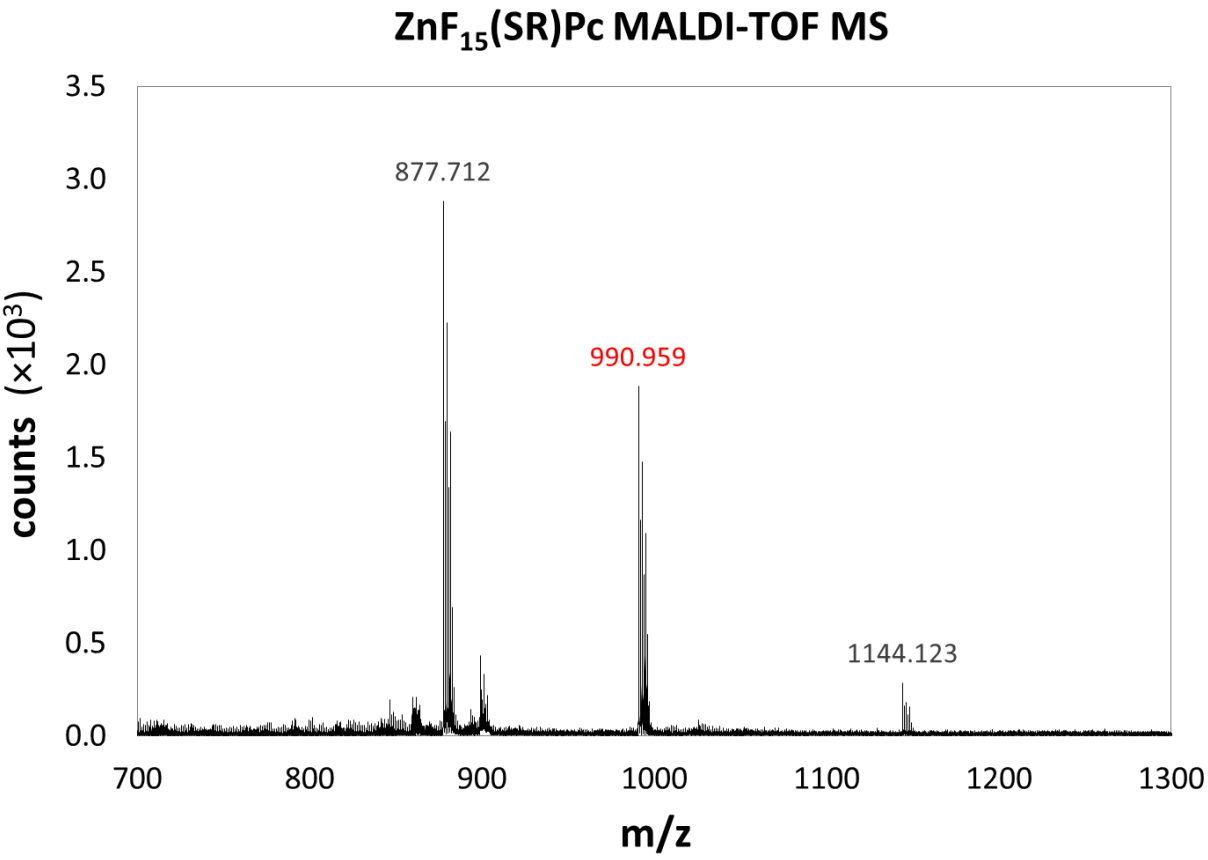

Structure	Observed Mass Range		Expected Mass Range	
$[ZnF_{15}(SH)Pc]^+$	877.71	883.77	877.91	883.90
$[ZnF_{15}(SR)Pc+H]^+$	990.96	997.04	991.04	997.04
$[ZnF_{12}(SR)_2(SH)_2Pc]^+$	1144.12	1150.12	1144.10	1150.10

Figure S8. Mass spectrum of zinc (II) octylthiopentadecafluorophthalocyanine ($ZnF_{15}(SR)Pc$) in a DHB matrix. A very small amount of fragmented tetra-substituted Pc also appears to be present, as well as significant fragmentation of the primary compound. The structural notation is described in detail above.

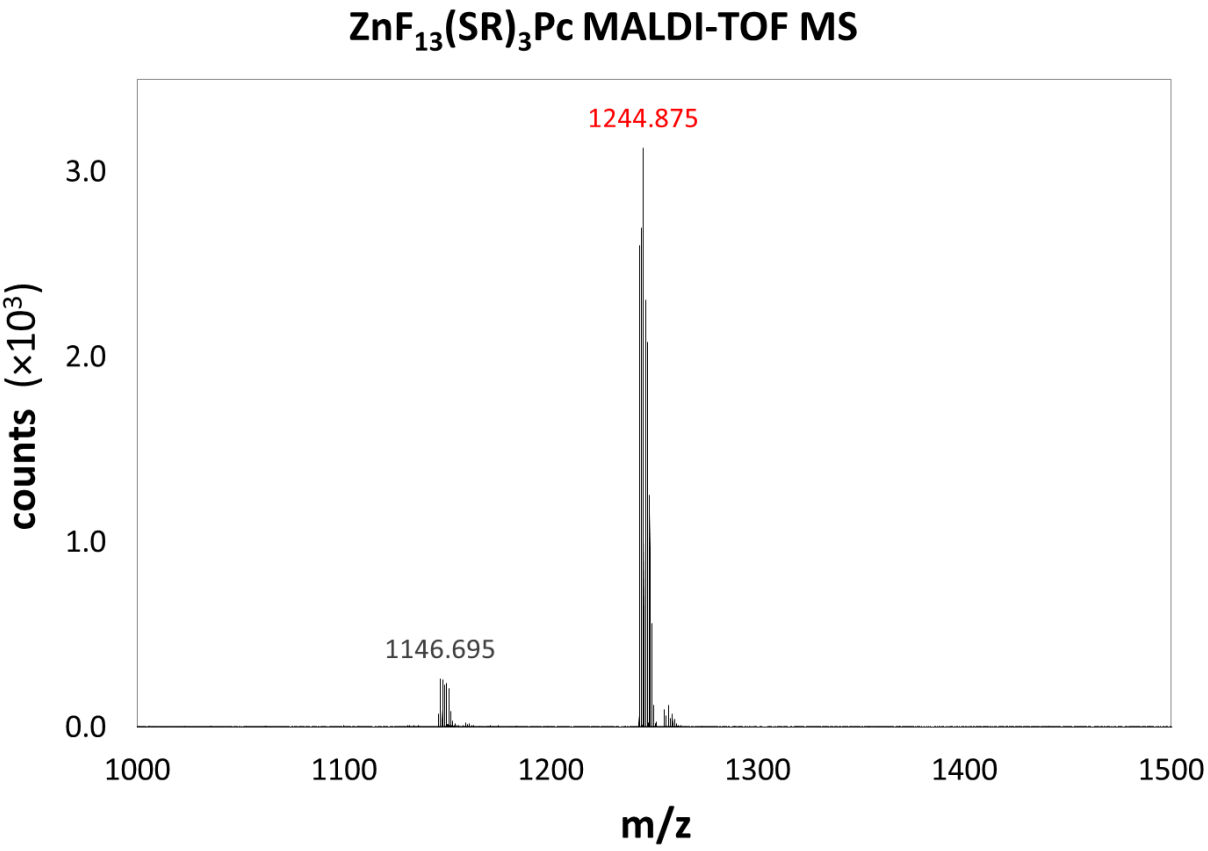

Structure	Observed Mass Range		Expected Mass Range	
$[ZnF_{13}(SH)_2(SH)OPc]^+$	1145.70	1153.74	1146.12	1153.11
$[ZnF_{13}(SR)_3Pc+H]^+$	1242.88	1249.90	1243.26	1250.25

Figure S9. Mass spectrum of zinc (II) tris(octylthio)tridecafluorophthalocyanine ($ZnF_{13}(SR)_3Pc$) in a DHB matrix. A small amount of an oxidized fragment ion is also present. The structural notation is described in detail above.

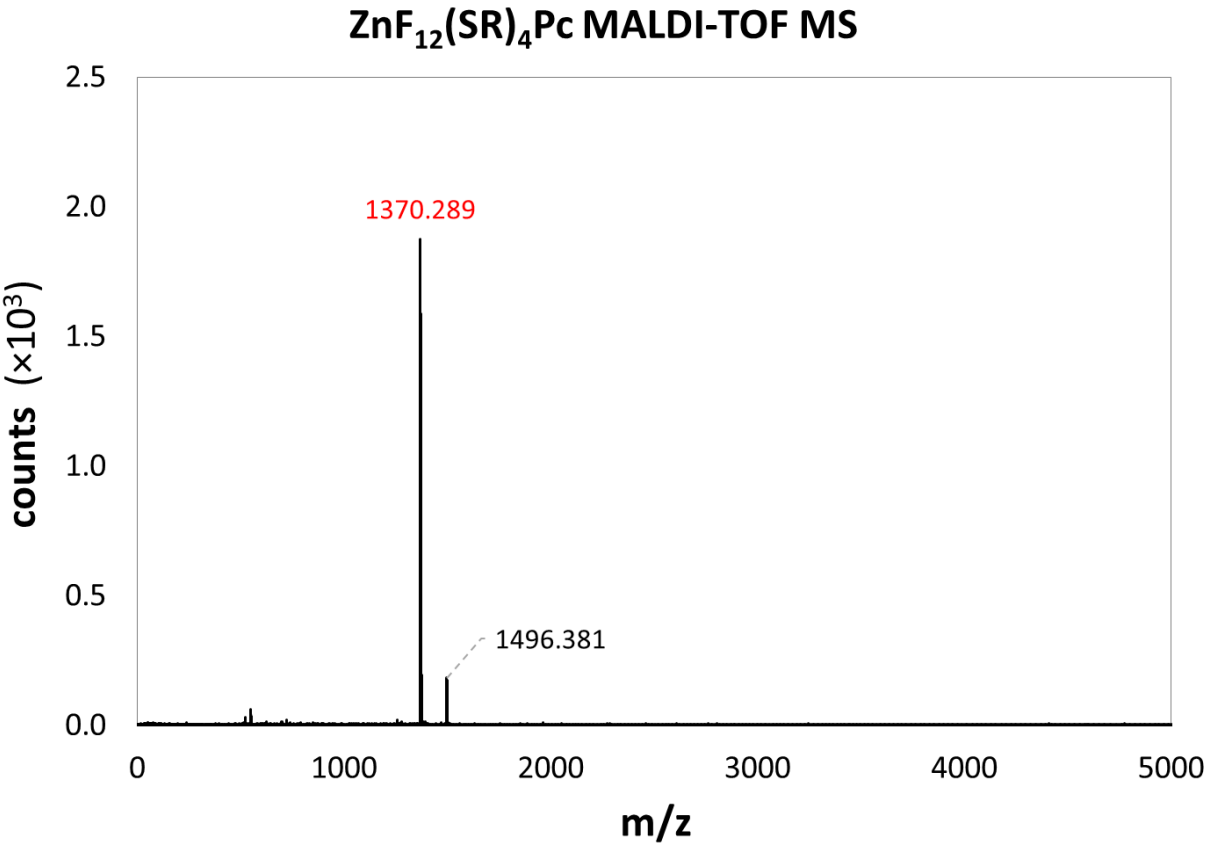

Structure	Observed Mass Range		Expected Mass Range	
$[ZnF_{12}(SR)_4Pc]^+$	1368.28	1376.31	1368.35	1376.35
$[ZnF_{11}(SR)_5Pc]^+$	1494.39	1501.37	1494.46	1501.47

Figure S10. Mass spectrum of zinc (II) tetrakis(octylthio)dodecafluorophthalocyanine ($ZnF_{12}(SR)_4Pc$) in a DHB matrix. A very small amount of the pentakis- substituted product is also present. The structural notation is described in detail above.

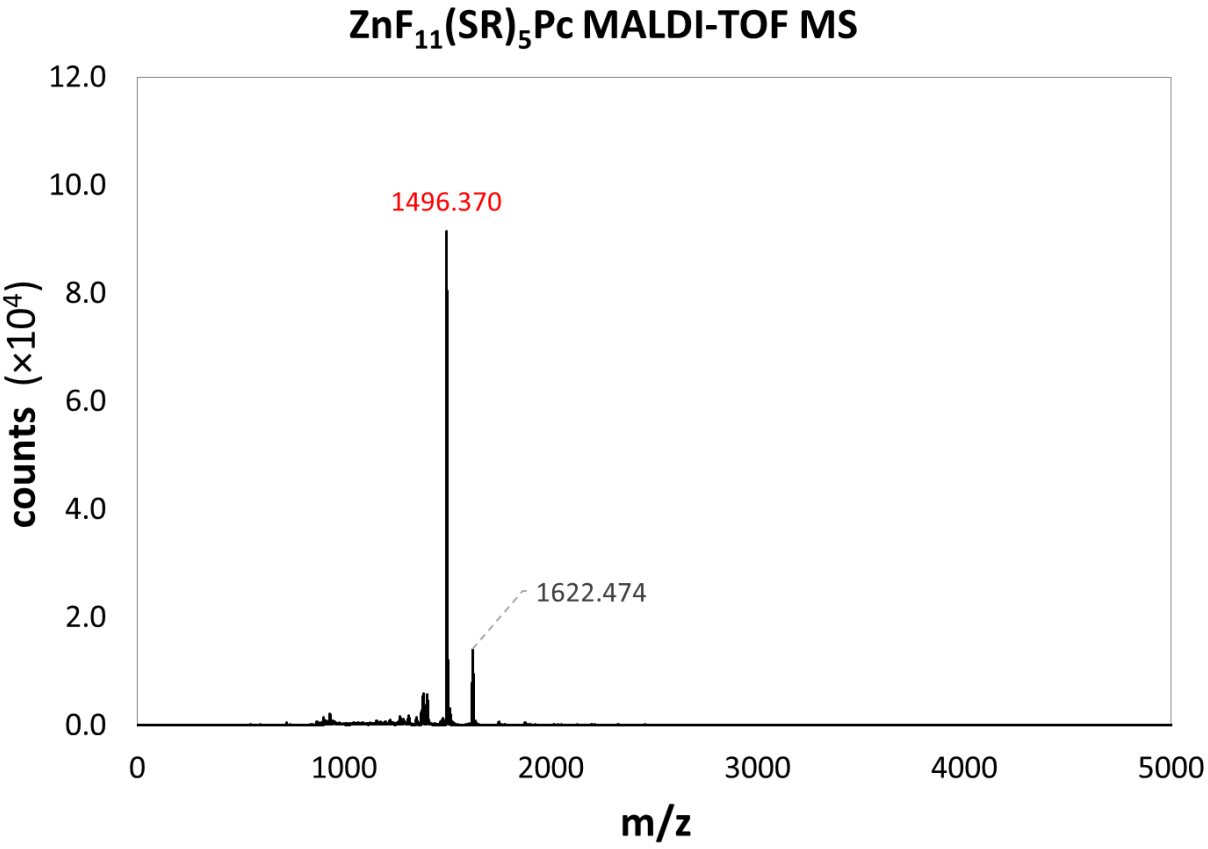

Structure	Observed Mass Range		Expected Mass Range	
$[ZnF_{11}(SR)_5Pc]^+$	1494.35	1503.42	1494.46	1501.47
$[ZnF_{10}(SR)_6Pc]^+$	1620.47	1628.48	1620.57	1629.57

Figure S11. Mass spectrum of Zinc (II) pentakis(octylthio)undecafluorophthalocyanine ($ZnF_{11}(SR)_5Pc$) in a DHB matrix. A very small amount of the hexakis- substituted product is also present. The structural notation is described in detail above.

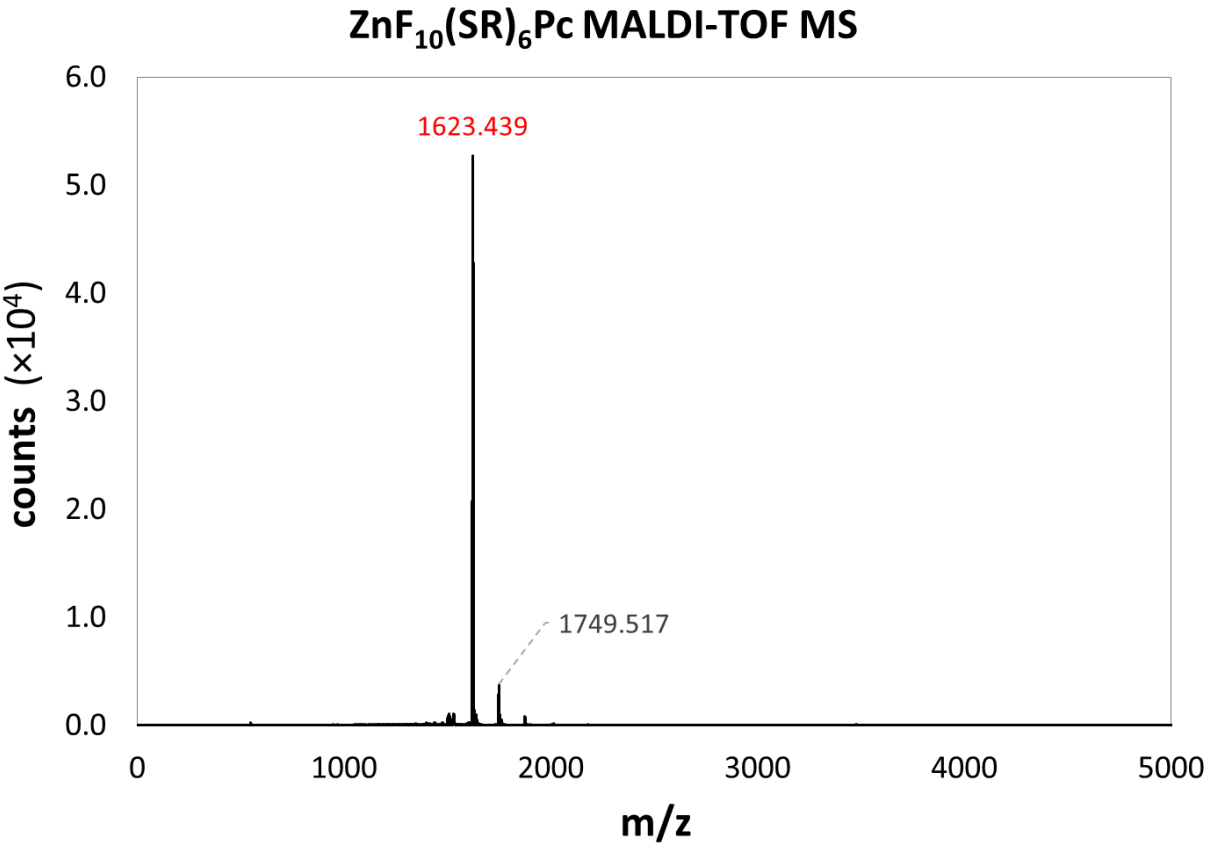

Structure	Observed Mass Range		Expected Mass Range	
$[ZnF_{10}(SR)_6Pc]^+$	1620.43	1629.44	1620.57	1629.57
$[ZnF_9(SR)_7Pc]^+$	1745.54	1754.51	1746.68	1755.68

Figure S12. Mass spectrum of Zinc (II) hexakis(octylthio)decafluorophthalocyanine ($ZnF_{10}(SR)_6Pc$) in a DHB matrix. A very small amount of the heptakis- substituted product is also present. The structural notation is described in detail above.

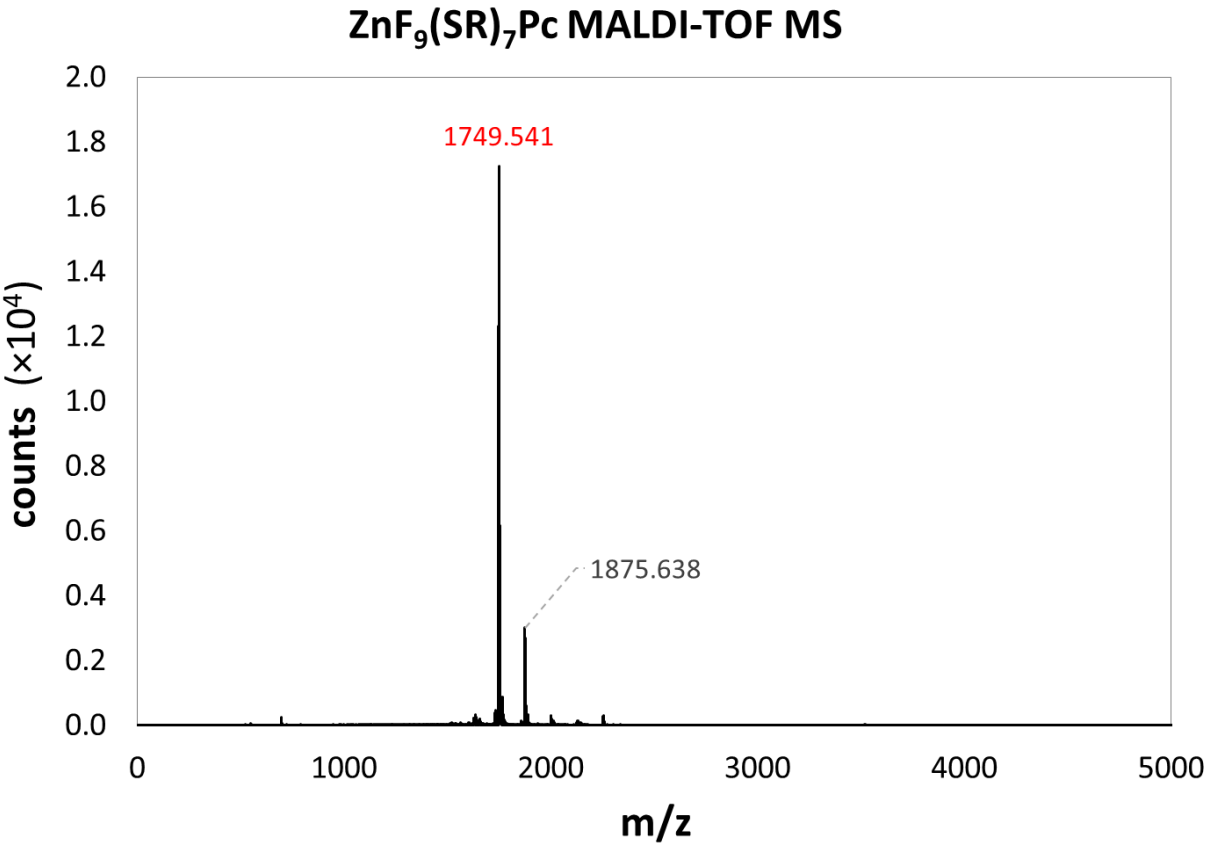

Structure	Observed Mass Range		Expected Mass Range	
$[ZnF_9(SR)_7Pc]^+$	1746.54	1755.56	1746.68	1755.68
$[ZnF_8(SR)_8Pc]^+$	1872.63	1881.64	1872.78	1882.78

Figure S13. Mass spectrum of Zinc (II) heptakis(octylthio)nonafluorophthalocyanine ($ZnF_9(SR)_7Pc$) in a DHB matrix. A very small amount of the octakis- substituted product is also present. The structural notation is described in detail above.

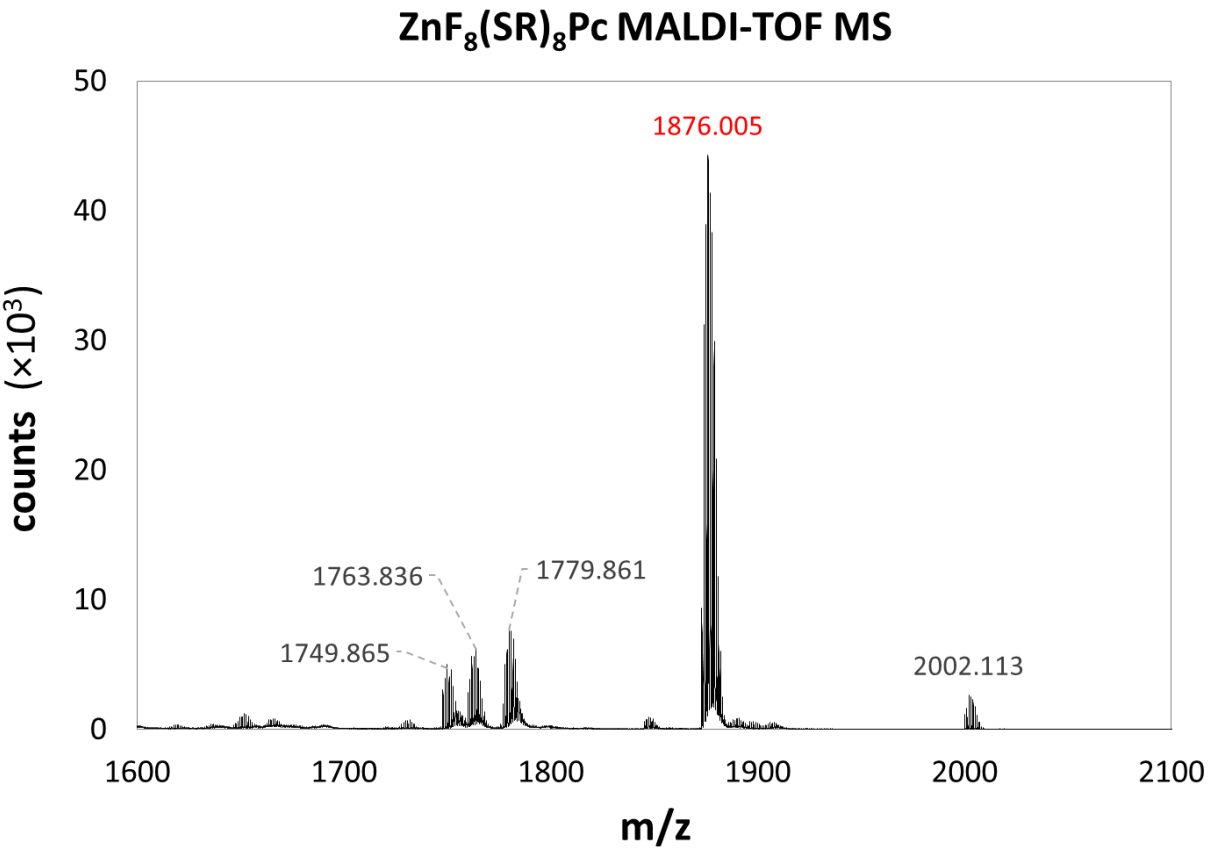

Structure	Observed Mass Range		Expected Mass Range	
$[ZnF_9(SR)_7Pc]^+$	1747.87	1755.06	1746.68	1755.68
$[ZnF_8(SR)_7(SH)Pc]^+$	1759.87	1767.88	1760.66	1769.66
$[ZnF_8(SR)_7(SH)OPc]^+$	1776.88	1784.86	1776.65	1785.65
$[ZnF_8(SR)_8Pc]^+$	1872.99	1882.98	1872.78	1882.78
$[ZnF_7(SR)_9Pc]^+$	2000.10	2009.14	1998.89	2008.88

Figure S14. Mass spectrum of Zinc (II) octakis(octylthio)octafluorophthalocyanine ($ZnF_8(SR)_8Pc$) in a DHB matrix. Some fragmentation and oxidation products are present, as well as very small amounts of the heptakis- and nonakis- substituted products. The structural notation is described in detail above.

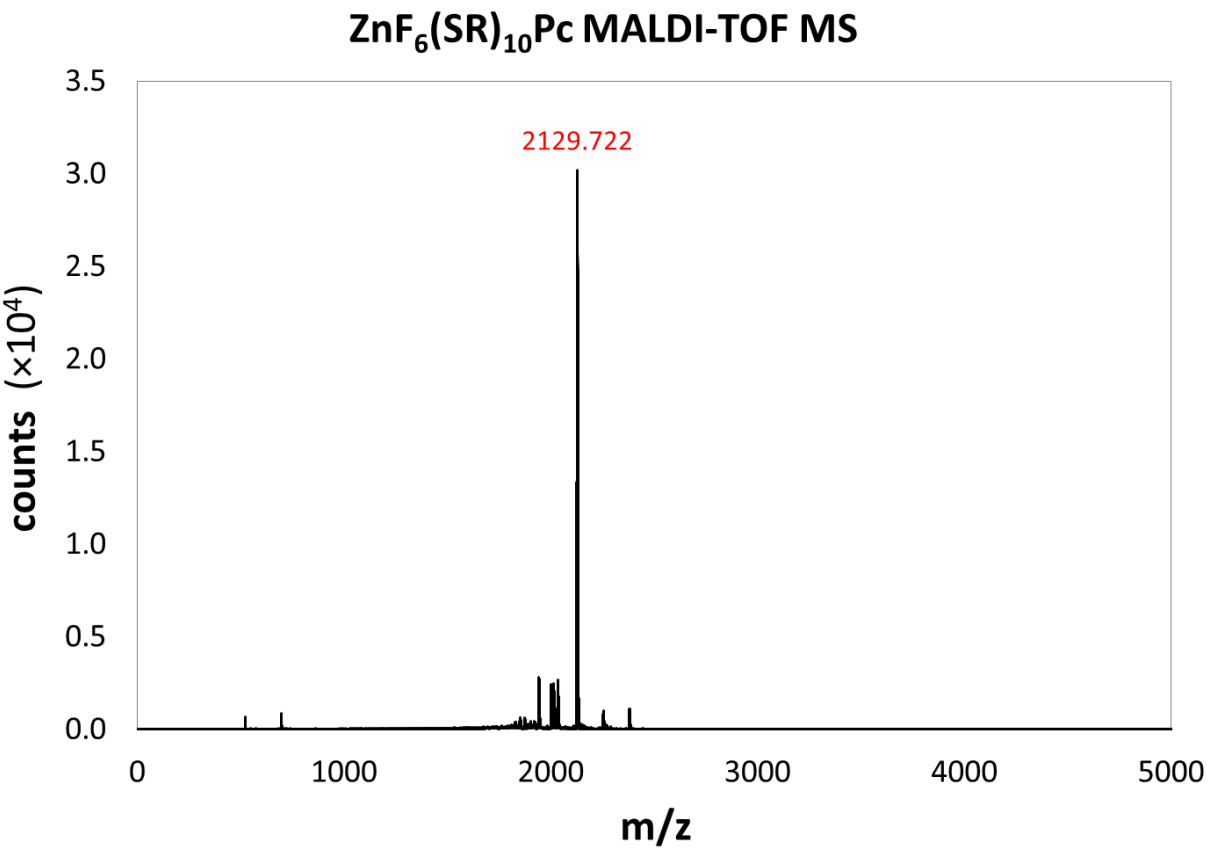

Structure	Observed Mass Range		Expected Mass Range	
$[ZnF_6(SR)_{10}Pc]^+$	2125.72	2135.74	2125.00	2134.00

Figure S15. Mass spectrum of Zinc (II) decakis(octylthio)hexafluorophthalocyanine ($ZnF_6(SR)_{10}Pc$) in a DHB matrix. Very small amounts of oxidized fragment ions are also present. The structural notation is described in detail above.

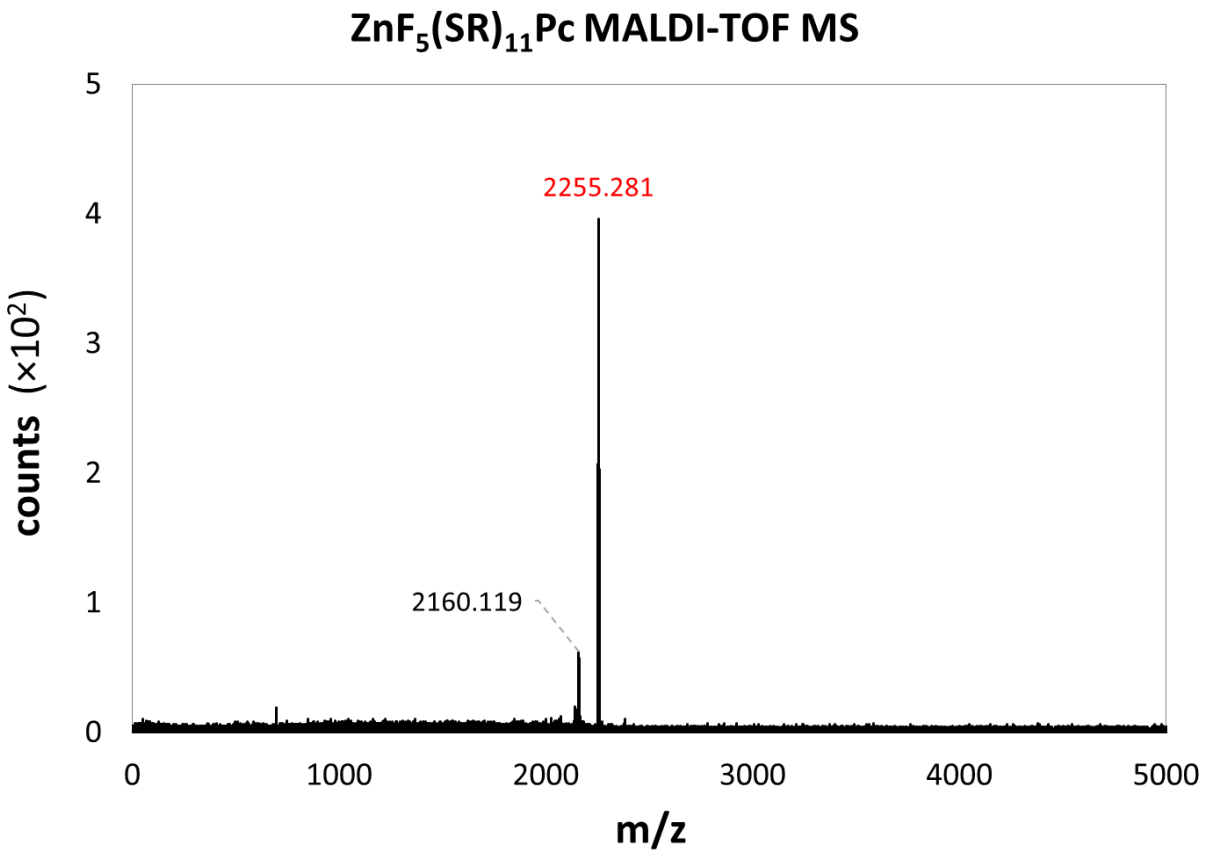

Structure	Observed Mass Range		Expected Mass Range	
$[ZnF_5(SR)_{10}(SH)OPc+H]^+$	2156.13	2165.22	2155.98	2165.97
$[ZnF_5(SR)_{11}Pc+H]^+$	2252.26	2260.27	2252.11	2262.10

Figure S16: Mass spectrum of Zinc (II) undecakis(octylthio)pentafluorophthalocyanine ($ZnF_5(SR)_{11}Pc$) in a DHB matrix. A small amount of an oxidized fragment ion is also present. The structural notation is described in detail above.

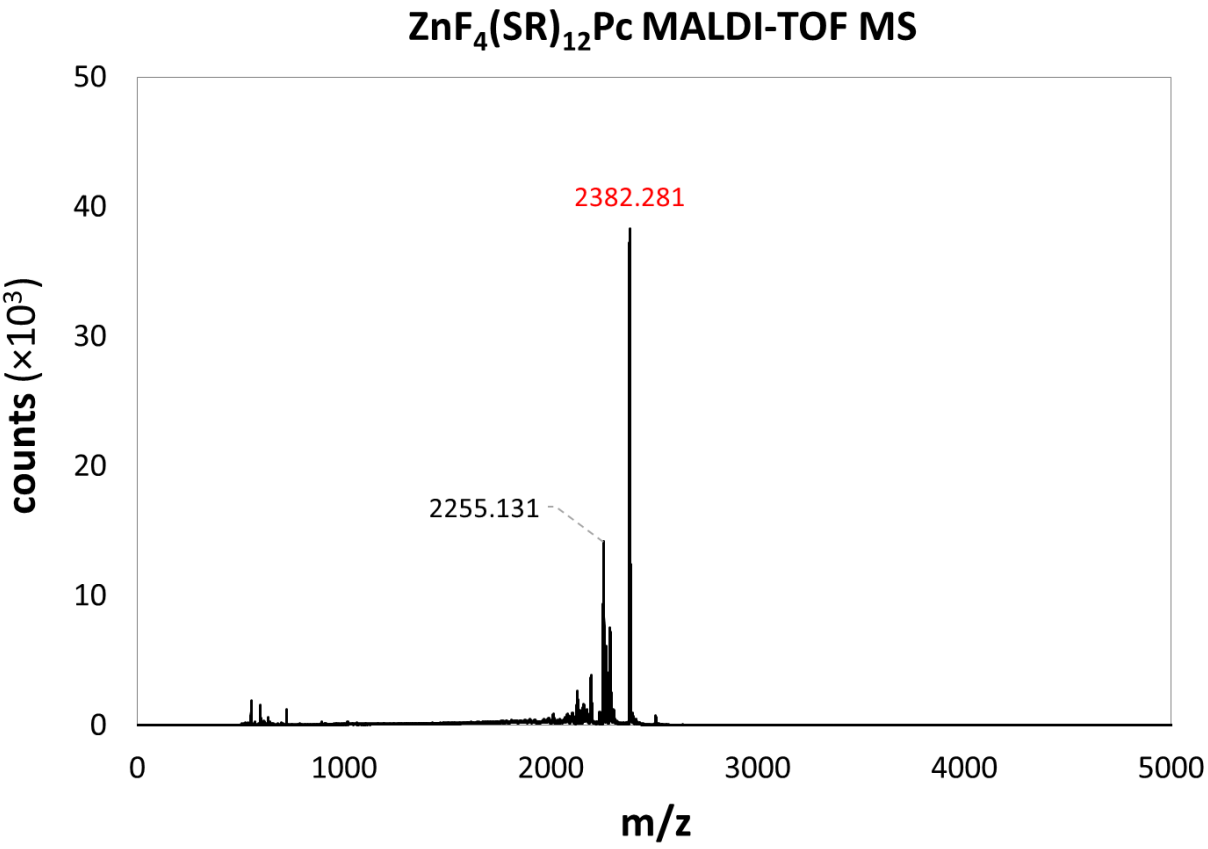

Structure	Observed Mass Range		Expected Mass Range	
$[ZnF_5(SR)_{11}Pc+H]^+$	2252.16	2262.19	2252.11	2262.10
$[ZnF_4(SR)_{12}Pc+H]^+$	2378.27	2388.29	2378.21	2388.21

Figure S17. Mass spectrum of Zinc (II) dodecakis(octylthio)tetrafluorophthalocyanine ($ZnF_4(SR)_{12}Pc$) in a DHB matrix. A small amount of the undecakis- substituted product is also present. The structural notation is described in detail above.

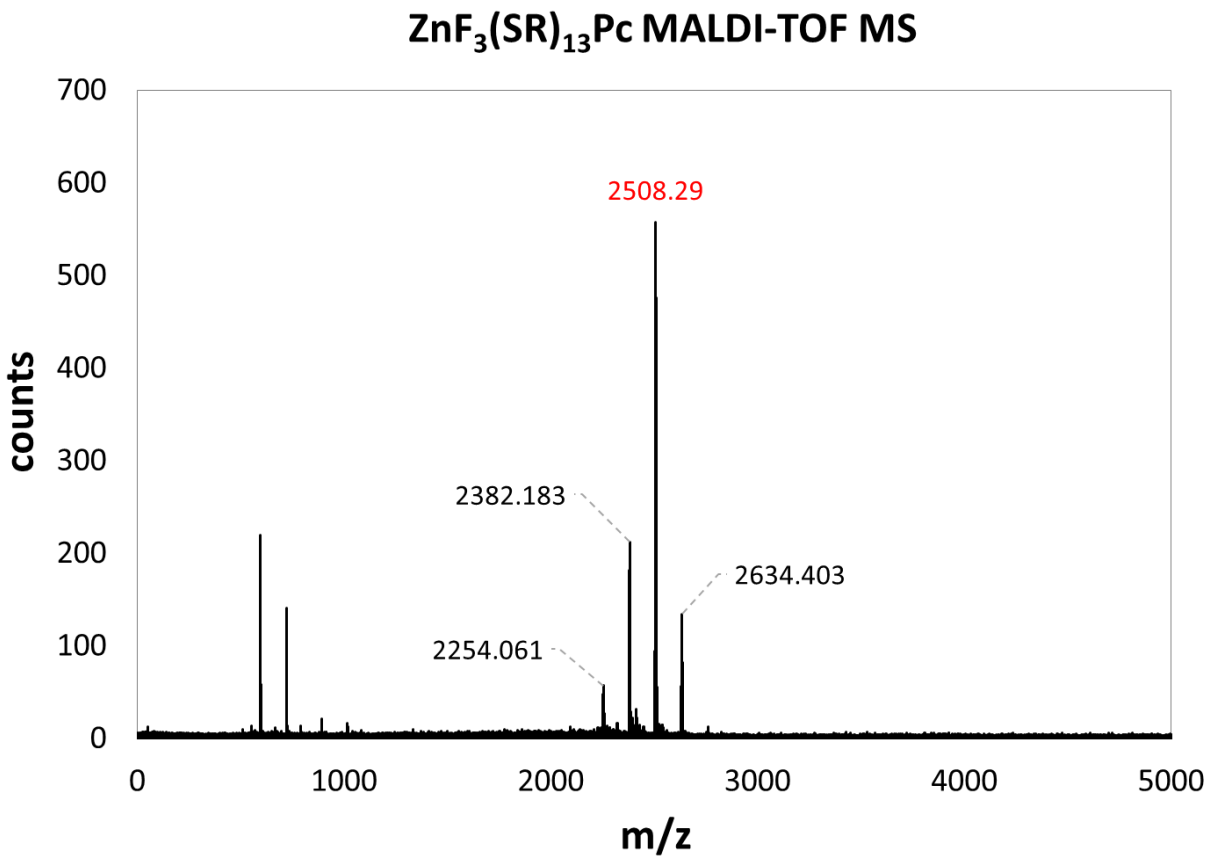

Structure	Observed Mass Range		Expected Mass Range	
$[ZnF_5(SR)_{11}Pc+H]^+$	2252.04	2261.16	2252.11	2262.10
$[ZnF_4(SR)_{12}Pc+H]^+$	2378.20	2388.15	2378.21	2389.22
$[ZnF_3(SR)_{13}Pc+H]^+$	2504.29	2513.27	2504.32	2515.31
$[ZnF_2(SR)_{14}Pc+H]^+$	2630.39	2639.42	2630.43	2642.42

Figure S18. Mass spectrum of Zinc (II) triskadecakis(octylthio)trifluorophthalocyanine ($ZnF_3(SR)_{13}Pc$) in a DHB matrix. Small amounts of the undecakis-, dodecakis-, and tetradecakis-substituted products are also present, as well as some unidentified smaller fragments. The structural notation is described in detail above.

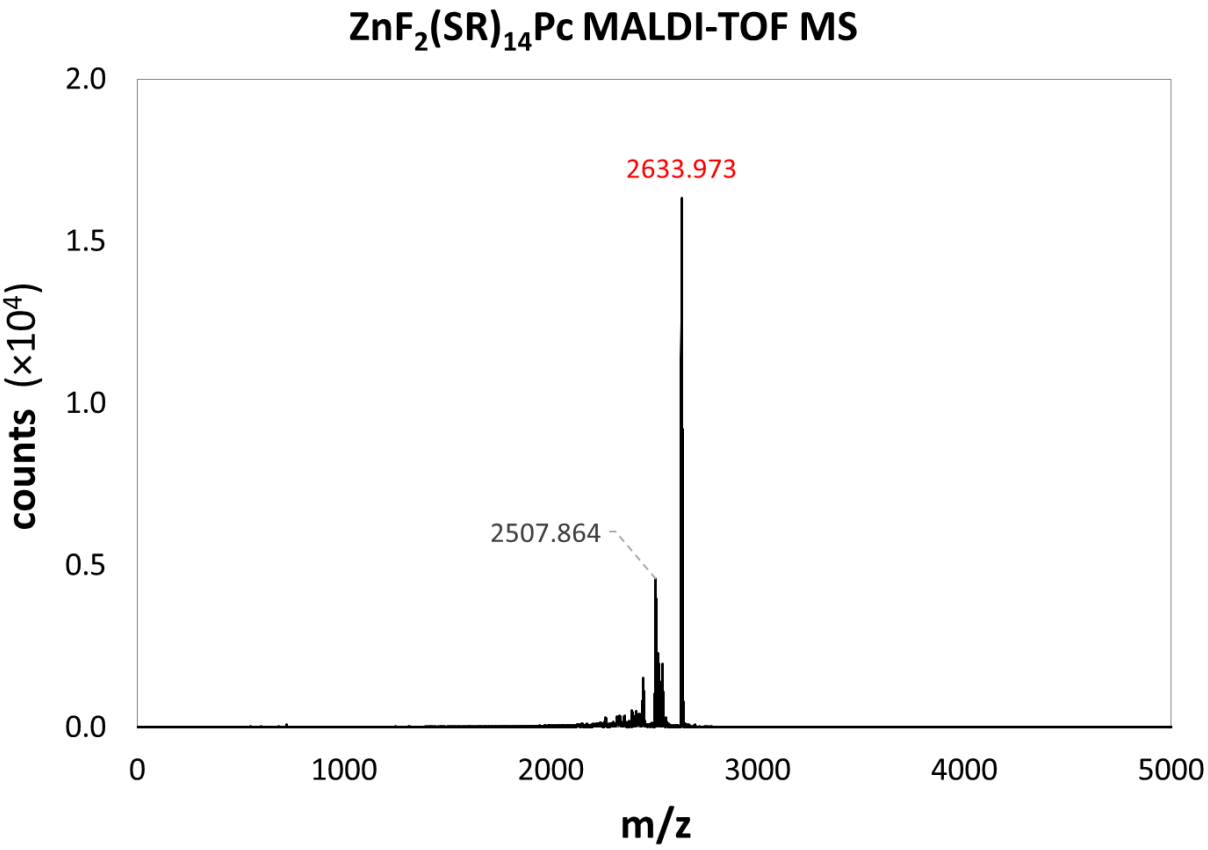

Structure	Observed Mass Range		Expected Mass Range	
$[ZnF_3(SR)_{13}Pc]^+$	2503.85	2513.86	2503.32	2514.31
$[ZnF_2(SR)_{14}Pc]^+$	2629.98	2640.98	2629.42	2641.42

Figure S19. Mass spectrum of Zinc (II) tetradecakis(octylthio)difluorophthalocyanine ($ZnF_2(SR)_{14}Pc$) in a DHB matrix. A small amount of the triskadecakis- substituted product is also presents. The structural notation is described in detail above.

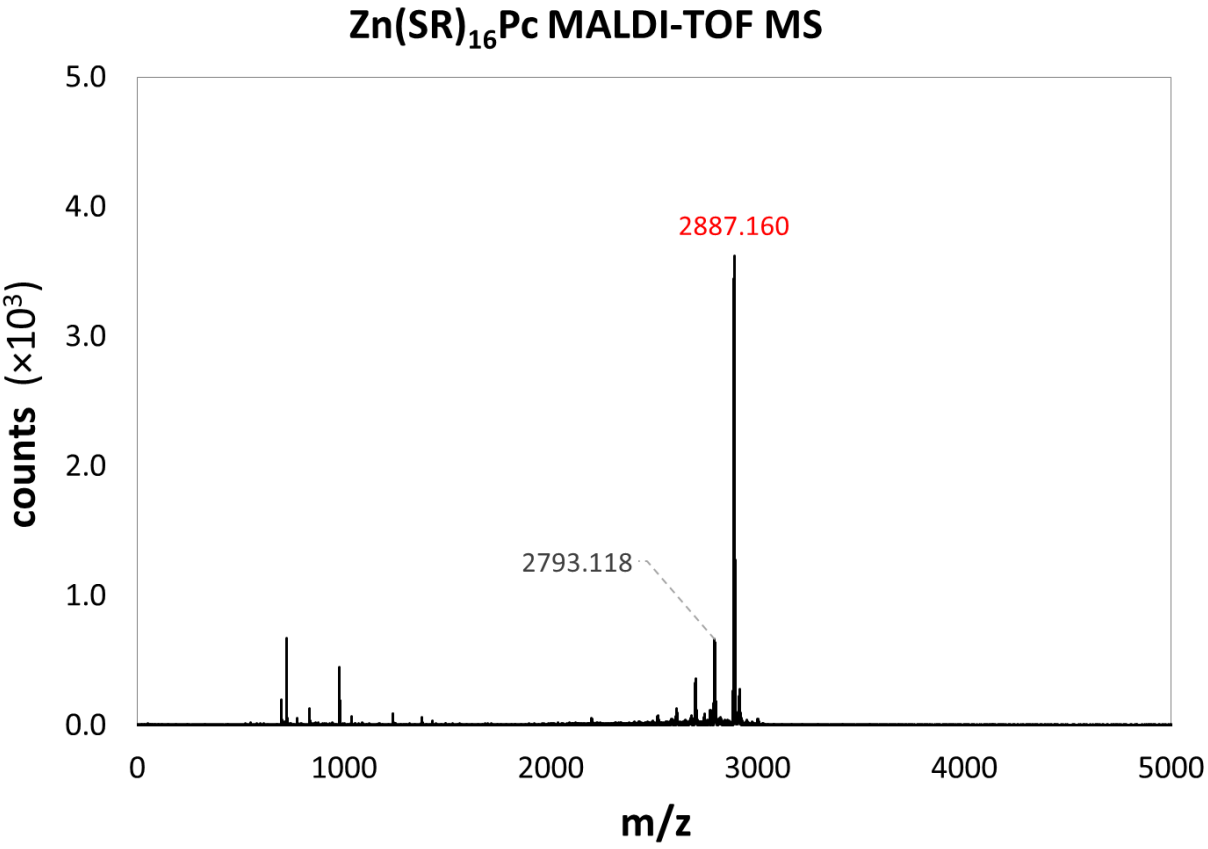

Structure	Observed Mass Range		Expected Mass Range	
$[Zn(SR)_{15}(SH)OPc]^+$	2789.12	2797.12	2786.50	2797.51
$[Zn(SR)_{16}Pc]^+$	2882.19	2894.17	2881.64	2893.64

Figure S20. Mass spectrum of Zinc (II) hexadecakis(octylthio)phthalocyanine ($Zn(SR)_{16}Pc$) in a DHB matrix. Small amounts of some oxidized fragments are also present. The structural notation is described in detail above.

Table S1. Electronic transitions for $ZnF_{16}Pc$, $ZnF_{12}(SR)_4Pc$-β, $ZnF_8(SR)_8Pc$-β, $ZnF_4(SR)_{12}Pc$-β, and $Zn(SR)_{16}Pc$, calculated by TD-DFT using the B3LYP hybrid exchange-correlation functional and the 6-31G(d,p) basis set.

Compound	λ^a	f^b	Wavefunction[c]
$ZnF_{16}Pc$	616	0.442	95% (H→L) + …
	613	0.444	95% (H→L+1) + …
	374	0.019	61% (H–5→L+1) + 34% (H–3→L) + …
	367	0.107	5% (H–9→L+1) + 30% (H–5→L+1) + 63% (H–3→L) + …
	366	0.144	6% (H–9→L) + 21% (H–5→L) + 67% (H–3→L+1) + …
$ZnF_{12}(SR)_4Pc$–β	644	0.562	96% (H→L) + …
	641	0.586	96% (H→L+1) + …
	458	0.044	10% (H–2→L) + 84% (H–2→L+1) + …
	456	0.093	7% (H–4→L) + 72% (H–2→L) + 9% (H–2→L+1) + 10% (H–1→L) + …
	441	0.110	88% (H–4→L) + 7% (H–2→L) + …
	436	0.119	94% (H–4→L+1) + …
	401	0.014	93% (H–8→L+1) + …
	383	0.164	93% (H–6→L) + …
	382	0.155	93% (H–6→L+1) + …
$ZnF_8(SR)_8Pc$–β	674	0.608	96% (H→L) + …
	661	0.641	95% (H→L+1) + …
	558	0.034	6% (H–1→L) + 92% (H–1→L+1) + …
	553	0.076	92% (H–1→L) + 6% (H–1→L+1) + …
	505	0.063	8% (H–4→L) + 87% (H–2→L) + …
	496	0.024	5% (H–2→L) + 87% (H–2→L+1) + …
	490	0.013	84% (H–4→L) + 6% (H–2→L) + 5% (H–2→L+1) + …
	479	0.017	97% (H–3→L+1) + …
	478	0.040	94% (H–4→L+1) + …
	454	0.014	21% (H–5→L) + 72% (H–5→L+1) + …
	453	0.011	44% (H–6→L) + 30% (H–5→L) + 21% (H–5→L+1) + …
	451	0.093	44% (H–6→L) + 46% (H–5→L) + …
	440	0.053	6% (H–8→L) + 85% (H–7→L) + …

	436	0.055	92% (H–6→L+1) + …
	428	0.062	6% (H–11→L+1) + 7% (H–8→L) + 80% (H–7→L+1) + …
	427	0.063	81% (H–8→L) + 7% (H–7→L) + 5% (H–7→L+1) + …
	413	0.015	6% (H–11→L) + 77% (H–8→L+1) + …
	382	0.089	12% (H-15→L) + 22% (H-10→L) + 51% (H-9→L) + 10% (H-9→L+1) + …
	381	0.012	83% (H-15→L) + 6% (H-9→L) + …
	378	0.017	22% (H-10→L) + 64% (H-9→L+1) + …
	376	0.049	30% (H-10→L) + 29% (H-10→L+1) + 25% (H-9→L) + …
	373	0.083	14% (H-10→L) + 62% (H-10→L+1) + 5% (H-9→L) + 10% (H-9→L+1) + …
	361	0.037	36% (H-14→L) + 14% (H-13→L) + 37% (H-12→L) + …
	354	0.187	6% (H-18→L) + 36% (H-14→L) + 25% (H-13→L) + 14% (H-13→L+1) + 6% (H-12→L+1) + …
	351	0.108	10% (H-13→L) + 31% (H-13→L+1) + 13% (H-12→L) + 29% (H-12→L+1) + …
$ZnF_4(SR)_{12}Pc$–β	705	0.492	95% (H→L) + …
	698	0.542	95% (H→L+1) + …
	605	0.020	8% (H–2→L) + 79% (H–1→L) + 10% (H–1→L+1) + …
	601	0.032	11% (H–2→L) + 79% (H–1→L+1) + …
	583	0.013	29% (H–3→L+1) + 13% (H–2→L) + 50% (H–2→L+1) + …
	536	0.066	94% (H–4→L) + …
	526	0.083	92% (H–4→L+1) + …
	484	0.021	94% (H–5→L) + …
	475	0.097	89% (H–5→L+1) + …
	469	0.034	12% (H–8→L) + 75% (H–6→L) + …
	459	0.024	28% (H–7→L) + 32% (H–7→L+1) + 26% (H–6→L+1) + …
	456	0.019	7% (H–9→L+1) + 33% (H–8→L) + 14% (H–8→L+1) + 28% (H–7→L) + 6% (H–6→L) + …
	454	0.021	13% (H–9→L) + 61% (H–8→L+1) + 6% (H–7→L+1) + 8% (H–6→L) + …
	452	0.032	12% (H–9→L) + 19% (H–9→L+1) + 18% (H–8→L) + 7% (H–8→L+1) + 9% (H–7→L) + 27% (H–7→L+1) + …
	449	0.063	6% (H–11→L) + 47% (H–9→L) + 9% (H–8→L) + 5% (H–8→L+1) + 16% (H–7→L) + 6% (H–7→L+1) + …
	444	0.046	6% (H–10→L+1) + 17% (H–9→L) + 49% (H–9→L+1) + 13% (H–8→L) + …
	442	0.033	33% (H-11→L) + 58% (H-10→L) + …
	441	0.033	19% (H-11→L) + 59% (H-10→L+1) + 9% (H-9→L+1) + …
	438	0.024	32% (H-11→L) + 25% (H-10→L) + 24% (H-10→L+1) + …
	429	0.030	88% (H-11→L+1) + …
	427	0.019	78% (H-12→L) + …

	416	0.016	18% (H-13→L+1) + 71% (H-12→L+1) + …
	402	0.016	8% (H-14→L+1) + 63% (H-13→L+1) + 23% (H-12→L+1) + …
	373	0.067	17% (H-19→L) + 9% (H-17→L) + 8% (H-16→L) + 11% (H-15→L) + 41% (H-14→L) + …
	362	0.042	8% (H-14→L) + 55% (H→L+5) + …
$Zn(SR)_{16}Pc$	700	0.476	93% (H→L) + …
	688	0.522	92% (H→L+1) + …
	615	0.025	48% (H–2→L) + 44% (H–1→L) + …
	604	0.022	9% (H–3→L) + 21% (H–2→L) + 16% (H–2→L+1) + 23% (H–1→L) + 26% (H–1→L+1) + …
	595	0.013	6% (H–3→L) + 69% (H–2→L+1) + 15% (H–1→L+1) + …
	593	0.017	77% (H–3→L) + 5% (H–2→L) + 11% (H–1→L+1) + …
	582	0.010	86% (H–3→L+1) + …
	575	0.010	85% (H–4→L) + 6% (H–3→L+1) + …
	557	0.028	5% (H–5→L) + 13% (H–5→L+1) + 80% (H–4→L+1) + …
	545	0.021	87% (H–5→L) + 6% (H–4→L+1) + …
	530	0.027	82% (H–5→L+1) + 11% (H–4→L+1) + …
	485	0.017	7% (H–9→L) + 5% (H–9→L+1) + 40% (H–7→L) + 36% (H–7→L+1) + …
	483	0.011	12% (H–10→L) + 17% (H–9→L+1) + 7% (H–8→L) + 7% (H–8→L+1) + 22% (H–7→L) + 6% (H–7→L+1) + 21% (H–6→L+1) + …
	481	0.024	24% (H–9→L) + 11% (H–8→L+1) + 40% (H–7→L+1) + 7% (H–6→L+1) + …
	476	0.023	19% (H–8→L) + 10% (H–8→L+1) + 51% (H–6→L+1) + …
	472	0.036	12% (H–10→L) + 28% (H–9→L) + 6% (H–9→L+1) + 21% (H–8→L) + 21% (H–7→L) + …
	460	0.055	6% (H-11→L+1) + 39% (H-10→L) + 7% (H-10→L+1) + 10% (H-9→L) + 6% (H-9→L+1) + 14% (H-8→L) + 7% (H-8→L+1) + …
	455	0.032	50% (H-11→L) + 37% (H-10→L+1) + …
	453	0.052	17% (H-11→L) + 38% (H-11→L+1) + 33% (H-10→L+1) + …
	438	0.017	8% (H-17→L) + 11% (H-14→L) + 8% (H-13→L) + 57% (H-12→L) + …
	431	0.022	12% (H-14→L+1) + 24% (H-13→L) + 42% (H-12→L+1) + …
	422	0.019	9% (H-14→L+1) + 41% (H-13→L+1) + 14% (H-12→L+1) + 23% (H→L+2) + …
	421	0.031	14% (H-13→L+1) + 7% (H-12→L) + 62% (H→L+2) + …

[a] Transition wavelengths in nanometers. Only transitions with energies below ~3.5 eV (>350 nm) are given.

[b] Calculated oscillator strengths. Only transitions with oscillator strengths greater than 0.01 are given.

[c] Excited state wavefunction, in terms of the contributions of single-excitations of the ground state Slater determinant. Only single-excitations with contributions greater than 5% are given. The HOMO is designated "H", the second HOMO is "H-1", *etc*. The LUMO is designated "L", the second LUMO is "L+1", *etc*.

References

(1) Williams, A. Loopless Generation of Multiset Permutations using a Constant Number of Variables by Prefix Shifts. *Proceedings of the Twentieth Annual ACM-SIAM Symposium on Discrete Algorithms* **2009**, 987-996.

(2) Golchoubian, H.; Hosseinpoor, F. Effective Oxidation of Sulfides to Sulfoxides with Hydrogen Peroxide under Transition-Metal-Free Conditions. *Molecules* **2007**, *12*, 304-311.

(3) Chidawanyika, W.; Nyokong, T. The synthesis and photophysicochemical properties of low-symmetry zinc phthalocyanine analogues. *J. Photochem. Photobiol., A Chem.* **2009**, *206*, 169-176.

(4) Garcia, A. M.; Alarcon, E.; Munoz, M.; Scaiano, J. C.; Edwards, A. M.; Lissi, E. Photophysical behaviour and photodynamic activity of zinc phthalocyanines associated to liposomes. *Photochem. Photobiol. Sci.* **2011**, *10*, 507-514.